# Lagrangian and Eulerian drag models that are consistent between Euler-Lagrange and Euler-Euler (two-fluid) approaches for homogeneous systems

S. Balachandar [*]

*Department of Mechanical and Aerospace Engineering, University of Florida, Gainesville, Florida 32611, USA*

The undisturbed flow of a particle is of fundamental importance since it controls both the undisturbed flow force and the perturbation force (which includes quasisteady, added-mass, and history forces). Here we use the pairwise interaction extended point particle framework to evaluate the undisturbed flow of each particle through superposition of the perturbation flow induced by all its neighbors. This approach allows calculation of various statistics related to undisturbed fluid velocity under conditions of both stationary and nonstationary particles. In a random distribution of stationary particles, while the macroscale undisturbed flow is slowly varying, the microscale undisturbed flow that arises due to the perturbation flow of neighbors varies substantially from one particle to another and this in turn leads to large variation in the hydrodynamic force exerted on the particles. The effect of particle motion is generally to increase the particle-to-particle variation in the undisturbed fluid velocity of the particles. We observe that this increase is greater for the transverse component than for the streamwise component. As a result, with increasing random particle motion, the distribution of undisturbed fluid-velocity fluctuation becomes isotropic. Three different normalized forces are defined: $\Phi^L$ is the Lagrangian normalized force on an individual particle suitable for application in a microscale-informed Euler-Lagrange simulation, $\Phi^E$ is the Eulerian normalized average force suitable for application in an Euler-Euler simulation, and $\Phi^{LE}$ is the Lagrangian normalized force on an individual particle suitable for application in the standard Euler-Lagrange simulation. We establish precise relations between these different definitions. The drag laws developed based on particle-resolved direct numerical simulation results and experiments are appropriate for application only as the Eulerian normalized average force. We introduce the force consistency relation and use it to obtain an expression for $\Phi^L$, which when applied to each particle and averaged over all the particles equals $\Phi^E$. The results are first obtained in the limit of stationary particles and then extended to the general case of nonstationary particles.

## I. INTRODUCTION

The three commonly used computational approaches in multiphase flow problems are the particle-resolved (PR), Euler-Lagrange (EL), and Euler-Euler (EE) simulations. Among these, the PR direct numerical simulations (DNSs) are the most accurate, since the governing Navier-Stokes equations for the fluid and the Newton-Euler rigid-body equations of motion for the particles, along with boundary conditions that couple their motion, are solved without making any additional

---

[*]bala1s@ufl.edu

closure or modeling assumption besides interparticle collision models. In contrast, the EL and EE approaches are necessarily approximate, since their governing equations are obtained by averaging or filtering the fundamental Navier-Stokes and Newton-Euler equations. The resulting averaged equations include additional terms that require closure modeling assumptions.

In the EL approach, if the dynamics of all the particles within the system are followed, then there is no averaging over the particulate phase. The fluid phase is averaged or filtered over a length scale that is typically an order of magnitude or more larger than the particle diameter. The filtering process removes the pseudoturbulent component of the fluid phase by averaging out the perturbation flow induced by all the boundary layers and wakes around the particles. Depending on the filter size, some of the ambient turbulence may be filtered out as well. Nevertheless, the details of fluid pressure and stress distribution around each particle are lost and as a result, force and torque on the particles cannot be directly computed. They must be modeled in terms of the particle and the filtered fluid motion. The force and torque represent the momentum exchange between the particle and the surrounding flow and therefore must be applied in reverse back on the fluid. The small-scale velocity fluctuations that have been filtered out in the averaging process contribute to subgrid stress, whose closure model must account for the effect of the filtered microscale fluid motion on the dynamics of the larger fluid scales. Thus, in the EL approach, the filtering of the fluid phase has important consequences in the governing equations of both the fluid and the particulate phases.

In the Euler-Euler approach not only the fluid phase is averaged or filtered over a length scale larger than the particle diameter. The particulate phase is also suitably averaged over this length scale and this results in a continuum representation for the particulate phase. Instead of the Newton-Euler equations of motion for the individual particles in the Lagrangian frame, we now have continuum equations for the collective dynamics of the locally averaged state of the particles in the Eulerian frame. Hence the EE approach is also known as the two-fluid approach. In the EE approach, the averaging of both phases introduces the need for additional closure models. Even the closure models of force and torque that account for interphase momentum coupling become more complex and must be distinguished from the force and toque models that are employed in the EL approach. This distinction will be a focus of the present paper.

To explore this further, let us consider an EL simulation and a companion EE simulation of the same problem. In the EL simulation, the simplest approach to evaluating the force on each particle is to use the standard drag relation that is based on the relative velocity between the particle and the interpolated fluid velocity evaluated at the particle location [1]. Several improvements to this basic closure have been advanced and widely used in EL simulations. Most relevant to the present discussion is the finite-volume-fraction correction. As the local volume fraction of particles increases, the finite-Reynolds-number correction of the standard drag can be augmented to accounted for the finite volume fraction [2–10].

The standard drag model and its improvements are designed to account for the net pressure and viscous stress effects of the perturbation flow induced by the particle. It is important to note that these models predict the force on a particle in terms of its undisturbed flow, which is the source of the perturbation flow the particle induces. However, in an EL simulation, we do not have direct access to the undisturbed flow of the particle. Only the macroscale flow is known and its value interpolated to the center of the particle is typically used to compute the force. While the macroscale part of the undisturbed flow is nearly the same for all the particles within an averaging volume, the microscale component of the undisturbed flow substantially varies from particle to particle. This microscale variation is both due to differences in the arrangement and motion of neighboring particles (i.e., pseudoturbulence) and due to the random nature of filtered subgrid turbulence. Several recent efforts [11–19] have focused on understanding and modeling the deterministic effect of pseudoturbulence. An alternate approach is to statistically account for subgrid turbulence in the drag models by modifying the undisturbed fluid velocity at the particle location (obtained from the EL simulation) with an additional stochastic component obtained with a Langevin model [20].

Therefore, in order to develop proper force and torque models, we must distinguish the following two different EL implementations. In the first, the fluid velocity at the particle is simply taken to

be the macroscale velocity interpolated to the particle center, which we call EL-mac. The second approach attempts to approximate the fluid velocity at the particle more accurately by accounting for the microscale contribution, either deterministically or stochastically using a Langevin model. In either case, since the microscale variation in undisturbed fluid velocity is taken into account, we will call this second approach EL-mic.[1]

In the companion EE simulation, since the motion of individual particles is not being tracked, particle-related Eulerian quantities, such as the particle volume fraction $\phi(\boldsymbol{x}, t)$ and the particle-velocity field $\boldsymbol{v}(\boldsymbol{x}, t)$, represent average properties that result from a spatial filter or average of the underlying Lagrangian quantities. The microstructural details of how the particles are randomly distributed in the neighborhood of a point $\boldsymbol{x}$ are not known in an EE simulation. The only available information is the average number density of particles in a neighborhood, expressed as the particle volume-fraction field. The actual distribution of particles within the averaging volume around the point $\boldsymbol{x}$ will be random. Thus, there is a fundamental difference in particle characterization between the EL and EE approaches. In the EL approach, the particles are characterized in a deterministic fashion, while in the EE approach the particle characterization is necessarily stochastic. Even within the stochastic framework, $\phi(\boldsymbol{x}, t)$ is only the leading-order description in a hierarchy of possible statistical information. Quantities beyond $\phi(\boldsymbol{x}, t)$ are needed to properly characterize any inhomogeneity or anisotropy in the local distribution of particles at the microscale. The above description applies to particle-velocity field $\boldsymbol{v}(\boldsymbol{x}, t)$ and to all other particle-related quantities (such as granular temperature field) as well. In other words, $\boldsymbol{v}(\boldsymbol{x}, t)$ represents only the average particle velocity and the actual velocity of individual particles within the filter volume will substantially vary from the average value.

Thus, there are fundamental differences in what aspects of the hydrodynamic force on the particles are being modeled in the EL-mac, EL-mic, and EE approaches. In the EL-mac approach, the force on an individual particle is calculated taking into account its velocity and the macroscale fluid velocity at the particle location as

$$\boldsymbol{F}_i = 3\pi\mu d(\boldsymbol{u}_{\mathrm{mac}@\mathrm{i}} - \boldsymbol{v}_i)\Phi^{LE}(\mathrm{Re}_{\mathrm{mac}@\mathrm{i}}, \phi_{@\mathrm{i}}), \tag{1}$$

where $\boldsymbol{F}_i$ is the force on the $i$th particle of diameter $d$. Here $\mu$ is the dynamic viscosity of the fluid, $\boldsymbol{v}_i$ is the particle velocity, and $\boldsymbol{u}_{\mathrm{mac}@\mathrm{i}}$ is the macroscale fluid velocity of the EL simulation interpolated to the location of the $i$th particle. Note that subscript $i$ denotes a Lagrangian quantity and subscript @$i$ denotes an Eulerian quantity evaluated at the particle location. The function $\Phi^{LE}$ is the correction to the Stokes drag and it depends on both the macroscale Reynolds number of the $i$th particle, which is evaluated as $\mathrm{Re}_{\mathrm{mac}@\mathrm{i}} = d|\boldsymbol{u}_{\mathrm{mac}@\mathrm{i}} - \boldsymbol{v}_i|/\nu$, and the particle volume fraction evaluated at the $i$th particle.

In the EL-mic approach, the force on an individual particle is again calculated as

$$\boldsymbol{F}_i = 3\pi\mu d(\boldsymbol{u}_{@i} - \boldsymbol{v}_i)\Phi^L(\mathrm{Re}_{@i}, \phi_{@i}). \tag{2}$$

However, the relative velocity of the $i$th particle is based on its velocity $\boldsymbol{v}_i$ and the undisturbed fluid velocity $\boldsymbol{u}_{@i}$. Here the undisturbed fluid velocity $\boldsymbol{u}_{@i}$ includes both the macroscale contribution $\boldsymbol{u}_{\mathrm{mac}@\mathrm{i}}$ and the microscale contribution from the perturbation flow of its neighbors and filtered subgrid turbulence. The particle Reynolds number is also calculated based on this more accurate relative velocity estimation.

---

[1]In this work we will assume EL and EE simulations to be sufficiently coarse grained. In other words, the filter width $\mathcal{L} \gg d$, the particle diameter. As a result, Eulerian average drag will be an average over many particles that lie within the averaging volume. The results of this paper thus will not directly apply to fine-grained EL and EE simulations whose grid size is comparable to particle diameter. Similarly, in the EL approach the macroscale velocity at the particle location will be taken to be not corrupted by self-induced perturbation. Otherwise, a self-induced correction must be applied to recover the proper macroscale velocity (see [21–28]).

In the EE approach, the mean hydrodynamic force on all the particles within the averaging volume around the point $\boldsymbol{x}$, denoted by $\boldsymbol{F}(\boldsymbol{x}, t)$, is of primary interest. The traditional approach has been to evaluate the average force $\boldsymbol{F}(\boldsymbol{x}, t)$ based on the local volume fraction $\phi(\boldsymbol{x}, t)$ and the average velocity difference $\boldsymbol{u}(\boldsymbol{x}, t) - \boldsymbol{v}(\boldsymbol{x}, t)$, where $\boldsymbol{u}(\boldsymbol{x}, t)$ is the macroscale fluid velocity and $\boldsymbol{v}(\boldsymbol{x}, t)$ is the average particle velocity (both are part of the EE solution). Here again the average drag is expressed as that according to Stokes drag law multiplied by the correction function as

$$\boldsymbol{F}(\boldsymbol{x}, t) = 3\pi\mu d[\boldsymbol{u}(\boldsymbol{x}, t) - \boldsymbol{v}(\boldsymbol{x}, t)]\Phi^E(\text{Re}(\boldsymbol{x}, t), \phi(\boldsymbol{x}, t)). \tag{3}$$

In the above, $\text{Re}(\boldsymbol{x}, t) = d|\boldsymbol{u}(\boldsymbol{x}, t) - \boldsymbol{v}(\boldsymbol{x}, t)|/\nu$ is the average particle Reynolds number based on the average relative velocity (see footnote[1]).

We first draw attention to the important fact that the functions $\Phi^L$, $\Phi^{LE}$, and $\Phi^E$ are not the same, as indicated by differences in their superscript. Superscript $L$ denotes its applicability in the EL-mic simulation, which like a PR simulation tends to account for subgrid turbulence in particle motion. Superscript $E$ denotes applicability for the EE approach and superscript $LE$ denotes applicability in the EL-mac approach, where the fluid information for particle motion remains averaged. Henceforth we will refer to $\Phi^L$, $\Phi^{LE}$, and $\Phi^E$ as

$$\Phi^L = \text{Lagrangian normalized drag}$$

$$\Phi^E = \text{Eulerian normalized average drag}$$

$$\Phi^{LE} = \text{macro} - \text{Lagrangian normalized drag.}$$

All three functions have been normalized by their respective Stokes drag, and it must be stressed that the definition of Stokes drag and therefore the normalization is different for the three functions.

The difference between $\Phi^L$, $\Phi^{LE}$, and $\Phi^E$ arises from their nonlinear dependence on the parameters: Reynolds number and volume fraction. As pointed out earlier, there is substantial variation in the relative velocity of the individual particles within the averaging volume, which results in a substantial variation in the Reynolds number. Furthermore, variation in the manner in which particles are distributed within the averaging volume contributes to volume-fraction variation [29,30]. As a result of these variations, if we were to calculate the force on each particle using the Lagrangian normalized drag $\Phi^L$ and then average over all the particles within the average volume, the resulting average force would not equal that obtained by evaluating $\Phi^L$ based on the average Reynolds number and volume fraction. This clearly illustrates why the Eulerian normalized average drag correlation $\Phi^E$ must necessarily be different from the Lagrangian counterpart $\Phi^L$. The Eulerian normalized average force $\Phi^E$ must additionally account for the variation in the Reynolds number and volume fraction within the averaging volume.

The difference between $\Phi^L$, $\Phi^{LE}$, and $\Phi^E$ has been recognized by developers of various drag correlations [7,10,31]. However, the difference has not been well appreciated in typical EL and EE simulations. Often the standard drag correlation with the same finite Reynolds number and volume-fraction correction is used in both the EL and EE simulations, although in the former to calculate the drag on an individual particle and in the latter to calculate the average drag. Also, the drag laws developed based on PR DNS results of flow over a stationary random array of particles [2,3,6,7,9,10] are fundamentally different from those developed based on experiments with freely sedimenting particles [4,5,8]. Their difference is due to the distribution of particle Reynolds number and volume fraction within the averaging volume. Nevertheless, these drag correlations are directly appropriate for application only in EE simulations, owing to their average nature. The goal of the paper is to establish firm theoretical relations between the Lagrangian and the Eulerian normalized drag relations (i.e., between $\Phi^L$, $\Phi^{LE}$, and $\Phi^E$) and relate them to commonly used drag relations obtained from simulations and experiments.

We advance a force consistency relation between the $\Phi^L$, $\Phi^{LE}$, and $\Phi^E$ that must be satisfied when they are properly defined. According to this consistency relation, $\Phi^L$, when properly applied to each particle based on its relative velocity and volume fraction and averaged over all the particles within the averaging volume, must equal $\Phi^E$ (for consistency between EL and EE approaches also

see [32]). Accordingly, while $\Phi^L$ is only a function of the particle's Reynolds number and volume fraction [as defined in (2)], not only $\Phi^E$ must be a function of the average Reynolds number and average volume fraction, but its parametrization must also include proper quantification of variation in particle Reynolds number and volume fraction within the averaging volume. A similar consistency condition exists between $\Phi^L$ and its macroscale counterpart $\Phi^{EL}$. Establishing these consistency relations and elaborating on them is an important goal of the paper.

A technical difficulty arises in estimating the distribution of Reynolds numbers that will be encountered within the averaging volume. The particle-velocity variation can be easily assessed in an EL simulation and can be obtained from the granular temperature equation in the case of an EE simulation. In comparison it is not easy to estimate the level of particle-to-particle variation in the undisturbed fluid velocity within the averaging volume. This difficulty is because only the macroscale component of the undisturbed fluid velocity is available in EL and EE simulations. In this work we overcome this difficulty with the use of the pairwise interaction extended point-particle (PIEP) model [11,12,33]. This model provides a rational approximation for the pseudoturbulence generated by the particles in terms of summation of superposable wakes of all the particles. The PIEP model thus allows for the accurate evaluation of undisturbed fluid velocity $\boldsymbol{u}_{@i}$ of all the particles with the inclusion of the microscale component.

Towards our goal of establishing the appropriate $\Phi^L$, $\Phi^{LE}$, and $\Phi^E$ correlations, the strategy we follow in this paper proceeds along the following steps.

*(a) Eulerian average drag of a stationary homogeneous system (Sec. III C).* We first take the drag laws developed based on PR DNS results of flow over a stationary random array of particles [2,3,6,7,9,10] to be the Eulerian normalized average force $\Phi_0^E$, where subscript 0 indicates stationary particles.

*(b) Lagrangian drag of individual particles in a stationary homogeneous system (Sec. IV E).* Then, using the consistency relation and the PIEP model to estimate the undisturbed fluid velocity of a stationary random array of particles, we obtain the corresponding Lagrangian normalized force correlation $\Phi_0^L$.

*(c) Lagrangian drag of individual particles in a nonstationary homogeneous system (Sec. IV E).* For lack of additional detailed information, we then make the assumption that for a given particle Reynolds number $\mathrm{Re}_{@i}$ and volume fraction $\phi_{@i}$, the Lagrangian normalized force $\Phi^L$ in a nonstationary system remains the same as that for stationary particles (i.e., we assume $\Phi^L = \Phi_0^L$). This assumption can be justified in cases when relative particle motion is not very rapid and therefore the timescale of particle rearrangement is long. Nevertheless, the validity of this assumption must be verified.

*(d) Eulerian average drag of a nonstationary homogeneous system (Sec. IV D).* As the final step, $\Phi^L$ is used to evaluate the force on each particle in a random array of particles undergoing random motion following Maxwellian statistics (here again the PIEP model is used to evaluate the undisturbed fluid velocity of each particle). By averaging the force on all the particles we obtain the Eulerian normalized average force $\Phi^E$ for nonstationary particles. For averaging volumes much larger than the particle size, we recognize the fact that $\Phi^{LE}$ will approach $\Phi^E$.

The two key quantitative results of the present study are as follows. (i) The Lagrangian normalized force correlation $\Phi_0^L$ given in Eq. (33) is consistent with the Tenneti *et al.* [7] Eulerian average normalized force correlation $\Phi_0^E$. Both these are appropriate only for the stationary system. (ii) The Eulerian average normalized force correlation $\Phi^E$ given in (41) extends the Eulerian average normalized force correlation to nonstationary systems. While these results are of fundamental importance, due to the restriction to the homogeneous distribution of particles, their impact on practical multiphase flow problems will be incomplete. Extension of the present study to inhomogeneous and anisotropic distributions of particles is essential to obtain a complete parametrization.

## II. FRAMEWORK

Let us consider a multiphase flow that at time $t$ consists of $N$ particles that are located at $\boldsymbol{x}_i$ with velocity $\boldsymbol{v}_i$ (where $i = 1, 2, \ldots, N$). From the Lagrangian distribution of particles an Eulerian volume-fraction field can be defined as

$$\phi(\boldsymbol{x}, t) = \int_{\Omega} G(\boldsymbol{x} - \boldsymbol{x}') I_p(\boldsymbol{x}', t) dV, \tag{4}$$

where the integral is over the entire volume occupied by the multiphase flow and $I_p$ is the particle indicator function which is equal to unity only in regions occupied by the particle and is otherwise zero in regions occupied by the fluid. In Eq. (4) $G(\boldsymbol{x} - \boldsymbol{x}')$ is the filter function that has been assumed to be homogeneous and has been properly normalized to yield $\int_{\Omega} G \, dV = 1$. The filter function is generally chosen to be a top-hat function or a Gaussian of width $\mathcal{L}$ and thus the filter operation smoothens or averages out all subgrid variations that are smaller than the filter scale $\mathcal{L}$. An Eulerian particle-velocity field can similarly be constructed from the Lagrangian particle-velocity information as

$$\boldsymbol{v}(\boldsymbol{x}, t) = \frac{1}{\phi(\boldsymbol{x}, t)} \int_{\Omega} G(\boldsymbol{x} - \boldsymbol{x}') I_p(\boldsymbol{x}', t) \boldsymbol{v}_{pr}(\boldsymbol{x}', t) dV, \tag{5}$$

where $\boldsymbol{v}_{pr}(\boldsymbol{x}', t) = \boldsymbol{v}_i$ if $\boldsymbol{x}'$ falls within the volume of the $i$th particle, with a similar definition applying for all other particles. The particle velocity $\boldsymbol{v}_{pr}(\boldsymbol{x}', t)$ is undefined if $\boldsymbol{x}'$ falls within the fluid volume. Thus, $\boldsymbol{v}(\boldsymbol{x}, t)$ is the average velocity of all the particles around the point $\boldsymbol{x}$ weighted by the filter function. A similar definition applies to other particle properties and (5) can be used to convert any Lagrangian quantity into an Eulerian field that has been smoothened over the length scale $\mathcal{L}$.

Let $\boldsymbol{u}_{pr}(\boldsymbol{x}, t)$ be the particle-resolved fluid flow around the particles. However, in EL and EE simulations we only have access to the macroscale flow, which can be formally defined through the filter operation as

$$\boldsymbol{u}(\boldsymbol{x}, t) = \frac{1}{1 - \phi(\boldsymbol{x}, t)} \int_{\Omega} G(\boldsymbol{x} - \boldsymbol{x}') I_f(\boldsymbol{x}', t) \boldsymbol{u}_{pr}(\boldsymbol{x}', t) dV, \tag{6}$$

where the fluid indicator function is the complement of the particle indicator function [i.e., $I_f(\boldsymbol{x}, t) = 1 - I_p(\boldsymbol{x}, t)$]. Also, the normalization is with the fluid volume fraction $1 - \phi(\boldsymbol{x}, t)$. While the particle-resolved velocity $\boldsymbol{u}_{pr}$ is defined only in the region outside the particles, provided $\mathcal{L} \gg d$, the filtered macroscale velocity $\boldsymbol{u}(\boldsymbol{x}, t)$ is smoothly defined over the entire volume of the multiphase flow.

In a typical EL or EE simulation, the Eulerian fields are discretized and defined on a three-dimensional grid. They can then be evaluated at the $i$th particle through interpolation as

$$\boldsymbol{u}_{\text{mac@i}} = \boldsymbol{u}(\boldsymbol{x}_i, t), \quad \phi_{@i} = \phi(\boldsymbol{x}_i, t). \tag{7}$$

Other derived quantities can be defined either as Lagrangian quantities of the $i$th particle or as Eulerian fields averaged over all the particles around the point $\boldsymbol{x}$. Foremost among the derived quantities is the macroscale Reynolds number. The Lagrangian and Eulerian macroscale particle

Reynolds numbers[2] are defined as

$$\mathrm{Re}_{\mathrm{mac@i}} = \frac{d|\boldsymbol{u}_{\mathrm{mac@i}} - \boldsymbol{v}_i|}{\nu},$$

$$\mathrm{Re}_{\mathrm{mac}}(\boldsymbol{x}, t) = \frac{d|\boldsymbol{u}(\boldsymbol{x}, t) - \boldsymbol{v}(\boldsymbol{x}, t)|}{\nu}. \tag{8}$$

The above two Reynolds numbers are termed macroscale with the subscript *mac*, since they are based on the macroscale fluid velocity either as interpolated to the *i*th particle as $\boldsymbol{u}_{\mathrm{mac@i}}$ or evaluated at $\boldsymbol{x}$ as $\boldsymbol{u}(\boldsymbol{x}, t)$. These definitions do not include the effect of the velocity perturbations induced by the particles at the microscale.

### A. Macroscale and microscale undisturbed flow of the *i*th particle

With the above preliminaries we now carefully address what determines the particle force and how best to parametrize it in both the Lagrangian and Eulerian frameworks. We first note that any parametrization of force on a particle (including the simplest Stokes drag) is in terms of the undisturbed flow. Undisturbed flow of the *i*th particle is defined as the flow that would exist in the absence of the *i*th particle but in the presence of all other particles. With this definition, we can distinguish the following flow fields

$$\boldsymbol{u}_{pr}(\boldsymbol{x}, t) = \text{particle resolved flow around all the particles}$$

$$\boldsymbol{u}(\boldsymbol{x}, t) = \text{macroscale flow in the presence of all the particles}$$

$$\boldsymbol{u}_{pr, \neq i}(\boldsymbol{x}, t) = \text{particle resolved flow without the ith particle}$$

$$\boldsymbol{u}_{\neq i}(\boldsymbol{x}, t) = \text{macroscale flow without the ith particle,}$$

where the macroscale flows are filtered versions of the PR flows and the last two flows are the same as the first, but without the presence of the *i*th particle. Figure 1(a) shows an example of $\boldsymbol{u}_{pr}(\boldsymbol{x}, t)$ obtained from a PR simulation plotted on a small section of a vertical plane passing through a periodic box containing a random distribution of monodispersed particles. Here the macroscale flow is from the left to the right of the box and the wake behind the particles can be clearly identified. Figure 1(b) shows the corresponding PR velocity field in the absence of particle marked *i* (which is shown by a dashed line). This flow field is $\boldsymbol{u}_{pr, \neq i}(\boldsymbol{x}, t)$ and it is nonzero at the location of the *i*th particle. In a multiphase flow consisting of $N$ particles, $N$ such PR flows can be constructed by removing one particle at a time. Thus, it will not be computationally possible to evaluate $\boldsymbol{u}_{pr, \neq i}(\boldsymbol{x}, t)$ for all *i* using PR DNS and an efficient approach to evaluating it using the PIEP model will be presented below.

In this example, the computational box is a triply periodic cube whose size normalized by the particle diameter is $(3\pi)^3$. The box contains about 160 randomly distributed particles at an average volume fraction of about 10%. We define the filter to be a box filter of size the same as the triply periodic cube and thus the macroscale flow $\boldsymbol{u}(\boldsymbol{x}, t)$ is a uniform flow. The undisturbed macroscale flow of the *i*th particle $\boldsymbol{u}_{\neq i}(\boldsymbol{x}, t)$ that results from box filtering of $\boldsymbol{u}_{pr, \neq i}(\boldsymbol{x}, t)$ will also be a uniform flow. Its magnitude will be slightly higher than $\boldsymbol{u}(\boldsymbol{x}, t)$, since it is in the presence of one fewer particle within the cubic box; however, due to the large number of particles within the box, we make the assumption $\boldsymbol{u}_{\neq i}(\boldsymbol{x}, t) \approx \boldsymbol{u}(\boldsymbol{x}, t)$.

---

[2]Here and everywhere else in this work the particle Reynolds number is defined in terms of fluid velocity within the distribution of particles. We caution that in some papers Reynolds number is defined in terms of superficial fluid velocity, which will be lower by the multiplicative factor $1 - \phi$.
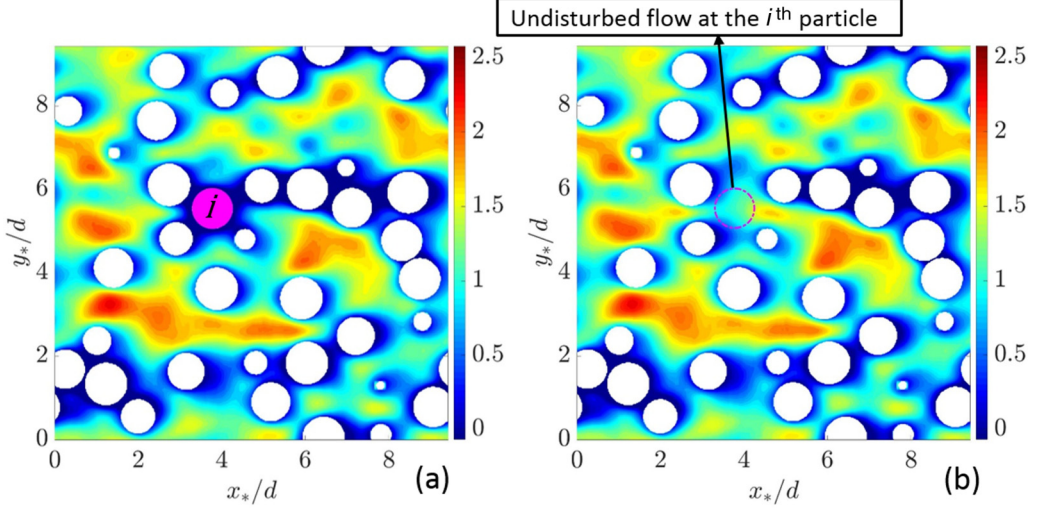
FIG. 1. (a) Contours of normalized streamwise velocity on a vertical plane computed in a particle-resolved simulation of flow around a random distribution of stationary particles in a periodic box. (b) Contours of normalized streamwise velocity on the same vertical plane in the absence of only the particle marked $i$. The resulting velocity field at the location of the $i$th particle is called the undisturbed velocity at the $i$th particle, whose complexity can be clearly associated with the perturbation flow induced by its neighbors. Both these flows were obtained by superposition of superposable wakes, which will be defined in Sec. II D.

Based on the above definitions, the undisturbed flow of the $i$th particle can thus be separated into macro and micro contributions as

$$\boldsymbol{u}_{pr,\neq i}(\boldsymbol{x},t) = \underbrace{\boldsymbol{u}(\boldsymbol{x},t)}_{\text{macro part}} + \underbrace{[\boldsymbol{u}_{pr,\neq i}(\boldsymbol{x},t) - \boldsymbol{u}(\boldsymbol{x},t)]}_{\text{micro part}=\boldsymbol{u}_{\text{mic,i}}(\boldsymbol{x},t)}, \tag{9}$$

where (i) the macroscale undisturbed flow accounts for the collective action of all the particles within the multiphase flow and (ii) the microscale undisturbed flow of the $i$th particle is given by the second term on the right-hand side and it accounts for the perturbation flow induced by the specific arrangement of all the neighbors of the $i$th particle. In general, the filter width is chosen such that the macroscale undisturbed flow varies negligibly from one particle to its nearby neighbor, while the microscale flow can dramatically change depending on the specific arrangement of the neighbors. In the example shown in Fig. 1(b), the microscale undisturbed flow of the $i$th particle is due to the perturbation velocity of all neighbors.

From the perspective of the $i$th particle we can separate the microscale perturbation flow induced by all the particles into two parts as

$$\underbrace{\boldsymbol{u}_{pr}(\boldsymbol{x},t) - \boldsymbol{u}(\boldsymbol{x},t)}_{\text{total perturbation}} = \underbrace{[\boldsymbol{u}_{pr,\neq i}(\boldsymbol{x},t) - \boldsymbol{u}(\boldsymbol{x},t)]}_{\text{neighbor perturbation}} + \underbrace{\boldsymbol{u}_{pr}(\boldsymbol{x},t) - \boldsymbol{u}_{pr,\neq i}(\boldsymbol{x},t)}_{\text{self-perturbation}}, \tag{10}$$

where the first term on the right-hand side is the perturbation flow due to all other particles and it is the same as the microscale undisturbed flow of the $i$th particles. The second term on the right-hand side is the perturbation flow induced by the $i$th particle in order to enforce its no-slip and no-penetration boundary conditions. As we will discuss in Sec. II C, this separation between self-induced and neighbor-induced perturbation flow is important in establishing the different forces that act on the $i$th particle.

### B. Reynolds number of the $i$th particle

For the evaluation of particle force, the undisturbed flow field must be evaluated "at" the $i$th particle. Based on the separation of the undisturbed flow velocity into its macroscale and microscale contributions we write

$$\boldsymbol{u}_{@i}(t) \approx \underbrace{\boldsymbol{u}(\boldsymbol{x}_i, t)}_{=\boldsymbol{u}_{\text{mac}@\text{i}}} + \underbrace{\boldsymbol{u}_{\text{mic,i}}(\boldsymbol{x}_i, t)}_{=\boldsymbol{u}_{\text{mic}@\text{i}}}. \tag{11}$$

The macroscale contribution can be directly evaluated from the computed flow field of the EL or EE simulation as given in (7). The microscale contribution $\boldsymbol{u}_{\text{mic}@\text{i}}$ is subgrid information and therefore is not directly available in EL and EE simulations. As will be discussed in Sec. II D, in an EL simulation, $\boldsymbol{u}_{\text{mic}@\text{i}}$ can be approximated from the knowledge of the relative location and motion of the neighboring particles, by modeling the neighbor-induced perturbation flow. In the EE approach, the microscale information of both the fluid and particle motion has been averaged, since the individual particles are not tracked. Nevertheless, the statistical influence of these microscale fluctuations in both the fluid and particle velocities remains important in the EE approach, whose modeling is the focus of this study.

As discussed before, the macroscale undisturbed flow varies slowly on the scale of the particle diameter and thus the definition of $\boldsymbol{u}_{\text{mac}@\text{i}}$ given in the above equation is adequate. However, this approximation is not appropriate for the microscale undisturbed flow. As can be seen in Fig. 1(b), the microscale flow varies substantially over the size of the particle. Thus, evaluating the microscale contribution at the center of the $i$th particle may not be adequate. A better estimation of the microscale undisturbed flow at the $i$th particle will be based on an average of the neighbor-induced perturbation flow over the surface of the $i$th particle as given by

$$\boldsymbol{u}_{\text{mic}@\text{i}} = \overline{(\boldsymbol{u}_{\text{mic,i}})}^{S_i}, \tag{12}$$

where $\overline{()}^{S_i}$ denotes an average over the surface of the $i$th particle. The motivation for this improved definition comes from Faxén's law [34] and its extension in the form of the Maxey-Riley-Gatignol equation. Though its use at finite Reynolds number and in the presence of multiple neighbors has not been rigorously established, we expect it to provide a better characterization of the undisturbed flow than evaluation at the center of the $i$th particle as given in (11).

Based on the above estimate of the undisturbed fluid velocity, the particle Reynolds number of the $i$th particle can be defined as

$$\text{Re}_{@i} = \frac{d|\boldsymbol{u}_{@i} - \boldsymbol{v}_i|}{\nu}, \tag{13}$$

which includes contributions from both the macroscale and microscale flows. Thus, in the rest of the paper we carefully distinguish the following two definitions of undisturbed flow and the corresponding Reynolds numbers: (i) $\boldsymbol{u}_{@i}$ and $\text{Re}_{@i}$ are the total undisturbed flow and Reynolds number, respectively [see Eqs. (11) and (13)], and (ii) $\boldsymbol{u}_{\text{mac}@\text{i}}$ and $\text{Re}_{\text{mac}@\text{i}}$ are the macroscale undisturbed flow and Reynolds number, respectively [see Eqs. (7) and (8)]. In contrast to the above two Reynolds-number definitions, the volume-fraction field has only the macroscale contribution and the definition of $\phi_{@i}$ for the average particle volume fraction at the $i$th particle given in (7) remains applicable.

### C. Undisturbed and perturbation flow forces on the $i$th particle

In relating the force on the $i$th particle to the undisturbed flow we distinguish the following two contributions. The first is the direct contribution and will be termed the undisturbed flow force. It is also often refereed to as the pressure gradient, stress divergence, or Archimedes force. This contribution is due to the net stress divergence that acts on the volume occupied by the particle and

is given by

$$\boldsymbol{F}_{un,i} \approx \underbrace{\mathcal{V}(-\boldsymbol{\nabla} p + \mu \nabla^2 \boldsymbol{u})_{@i}}_{=\boldsymbol{F}_{\text{mac,un,i}}} + \underbrace{\mathcal{V}\overline{(-\boldsymbol{\nabla} p_{\text{mic,i}} + \mu \nabla^2 \boldsymbol{u}_{\text{mic,i}})}^{V_i}}_{=\boldsymbol{F}_{\text{mic,un,i}}}, \tag{14}$$

where $\mathcal{V}$ is the volume of a particle and $\overline{(\,)}^{V_i}$ corresponds to an average over the volume of the $i$th particle. Here again, in the first term on the right-hand side, the macroscale contribution has been approximately evaluated at the center of the $i$th particle, due to the slow variation of the macroscale flow. In the second term, the volume average Faxén form is used for the microscale contribution. Even in the absence of the $i$th particle, the undisturbed flow force is experienced by the fluid that occupies the volume of the $i$th particle.

In the presence of the $i$th particle, the actual flow in the neighborhood of the particle will negotiate around the particle and result in the self-induced perturbation flow [see Eq. (10)]. The self-induced perturbation flow results in the second contribution, the perturbation flow force on the $i$th particle. As illustrated by the Basset-Boussinesq-Oseen and the Maxey-Riley-Gatignol equations, the perturbation flow force can further be divided into (i) the quasisteady force that depends on the relative velocity, (ii) the added-mass force, and (iii) the viscous history force, where (ii) and (iii) depend on the relative acceleration between the particle and the undisturbed flow [1,35,36].

Here we will restrict attention to nonaccelerating condition and focus on the approximation of the force on the $i$th particle

$$\boldsymbol{F}_i \approx \boldsymbol{F}_{\text{mac,un,i}} + \boldsymbol{F}_{\text{mic,un,i}} + \boldsymbol{F}_{\text{qs,i}}, \tag{15}$$

where the quasisteady force $\boldsymbol{F}_{\text{qs,i}}$ accounts for the effect of self-perturbation arising from both the macro and micro components of the undisturbed flow. In fact, the self-induced perturbation flow due to the $i$th particle will depend not only on the undisturbed flow of the $i$th particle, but also on the presence and the motion of the neighboring particles. Thus, even the quasisteady force due to the macroscale undisturbed flow will be influenced by the microscale details of how the neighbors are arranged around the $i$th particle.

The micro portion of the undisturbed flow force can be evaluated only in an EL-mic simulation and that too only approximately with the use of the PIEP model. In both the EL-mac and EE approaches, $\boldsymbol{F}_{\text{mic,un,i}}$ cannot be directly calculated. Therefore, in order to establish consistent relations between the force expressions of the three approaches, we will consider parametrization of the total force $\boldsymbol{F}_i$ as a modified quasisteady force that includes the macro and micro portions of the undisturbed flow force. A discussion of the parametrization of the undisturbed flow force alone in the EL and EE approaches is given in Appendixes A–C.

### D. Superposable wake approximation of the microscale flow

In both the EL and EE approaches, only the macroscale flow $\boldsymbol{u}$ is being computed and therefore there is no direct access to the microscale undisturbed flow $\boldsymbol{u}_{\text{mic,i}}$ of the $i$th particle. However, as shown in [33,37] the microscale undisturbed flow of the $i$th particle can be approximated as a sum over perturbation flow induced by each of the $N - 1$ neighbors taken one at a time to obtain

$$\boldsymbol{u}_{\text{mic,i}}(\boldsymbol{x}, t) \approx \sum_{j=1}^{N-1} \boldsymbol{u}_{sw}(\boldsymbol{x} - \boldsymbol{x}_j; \text{Re}_{@j}, \phi_{@j}), \tag{16}$$

where the perturbation flow of each neighbor is taken to be given by its superposable wake (denoted by the subscript $sw$). The superposable wake flow depends not only on the distance from the perturbing $j$th neighbor, but also on the Reynolds number of the flow and the average particle volume fraction at the neighbor. As discussed in [33,37], the superposable wakes are axisymmetric flows and have been precomputed and stored for varying values of $\text{Re}_{@j}$ and $\phi_{@j}$.

In the evaluation of the microscale undisturbed flow surface averaged over the surface of the $i$th particle we make the approximation

$$\boldsymbol{u}_{\text{mic@i}} = \overline{(\boldsymbol{u}_{\text{mic,i}})}^{S_i} \approx \sum_{j=1}^{N-1} \overline{(\boldsymbol{u}_{sw})}_j^{S_i}. \tag{17}$$

Due to the axisymmetric nature of the superposable wake, the surface average depends only on the axial and radial distance between the $i$-$j$ particle pair and on $\text{Re}_{@j}$ and $\phi_{@j}$, which determine the superposable wake. Axisymmetric maps of streamwise and transverse components of $\overline{(\boldsymbol{u}_{sw})}_j^{S_i}$ are precomputed and stored for varying values of $\text{Re}_{@j}$ and $\phi_{@j}$. For each particle, the appropriate contributions from its neighbors to the above sum are then read from the maps and added to obtain the microscale undisturbed velocity. As a final point, it should be noted that the above sums need not be carried out for all $N - 1$ neighbors. The superposable wake maps decay rapidly and are nearly zero when the distance between the $i$th and the $j$th particle exceeds more than a few particle diameters [33,37]. So, for each particle, the above sums need to include only the few nearest neighbors that fall within a distance of a few particle diameters.

### E. Quasisteady force parametrization in the EL approach

In our quest to parametrize the particle force, we will consider the three contributions listed in (15) and address how their sum can be modeled in the EL approach. We normalize the total force by the corresponding Stokes drag based on the undisturbed relative velocity as

$$\Phi^L = \frac{\boldsymbol{F}_i}{3\pi \mu d(\boldsymbol{u}_{@i} - \boldsymbol{v}_i)}, \tag{18}$$

where superscript $L$ denotes its applicability to each individual particle in an EL simulation. The $\Phi^L$ will depend on the following nondimensional factors: Reynolds number $\text{Re}_{@i}$, which is a nondimensional measure of relative velocity between the $i$th particle and its undisturbed ambient flow; volume fraction $\phi_{@i}$, which measures the average number density of particles around the $i$th particle; the relative location of all the other particles in relation to the $i$th particle measured as $(\boldsymbol{x}_j - \boldsymbol{x}_i)/d$ for $j = 1, 2, \ldots, i - 1, i + 1, \ldots, N$; and the relative velocity of the neighboring particles measured in terms of their Reynolds numbers $\text{Re}_{@j}$.

The above-listed dependences are more complex than how $\Phi^L$ is traditionally modeled. In the traditional approach, considerable simplification is achieved by limiting attention to only the average statistical influence of neighbors. This simplification leads to the EL-macro model $\Phi^{LE}$. At this simplified level, the collective influence of neighbors is accounted for through the volume fraction. The precise location of the neighbors and their motion are ignored in evaluating the undisturbed flow of the $i$th particle. This simplification greatly reduces the dependence and $\Phi^{LE}$ is modeled as a function of only $\text{Re}_{\text{mac@i}}$ and $\phi_{@i}$.[3]

However, there is ample evidence that the simpler parametrization based on only $\text{Re}_{\text{mac@i}}$ and $\phi_{@i}$ is not of sufficient accuracy [11,14–16,19]. It only accounts for the macroscale effects. Subgrid variation in both particle relative velocity and local particle volume fraction strongly influences the particle force. The complete dependence list presented above is needed to properly account for the following two influences of the neighbors: (i) the effect of the precise arrangement of neighbors around the $i$th particle in influencing the undisturbed flow at the $i$th particle, which can be taken into account through the definition of $\text{Re}_{@i}$ by including the microscale flow induced by the neighbors [see Eqs. (11)–(13)], and (ii) the effect of neighbors on the perturbation flow induced by the $i$th particle and therefore on the perturbation flow force. The latter effect requires the position and

---

[3]It should noted that at this level of simplification, $\boldsymbol{u}_{@i}$ in the denominator of (18) must be consistently approximated as $\boldsymbol{u}_{\text{mac@i}}$, without the microscale contribution.

velocity of the neighbors to be included in the complete list of dependences. However, because of a lack of detailed information, we will ignore the latter influence of neighbors and pursue force parametrization based on only $\mathrm{Re}_{@i}$ and $\phi_{@i}$.

### F. Force parametrization in the EE approach

Due to the additional averaging of the particulate phase, force parametrization in the EE approach is more challenging. In the EE approach, force on an individual particle is not the object of interest. We are interested in the average drag on all the particles in the neighborhood of a point $x$ weighted by the filter function. We again consider the three contributions listed in (15) and address how their sum is modeled in the EE approach. The total force normalized by the corresponding Stokes drag based on the macroscale undisturbed relative velocity is defined as

$$\Phi^E = \frac{\boldsymbol{F}(\boldsymbol{x},t)}{3\pi\mu d[\boldsymbol{u}(\boldsymbol{x},t) - \boldsymbol{v}(\boldsymbol{x},t)]}, \tag{19}$$

where superscript $E$ denotes its applicability in the EE approach. The Eulerian force field is defined as the weighted sum over all the particles within the system

$$\boldsymbol{F}(\boldsymbol{x},t) \approx \sum_{i=1}^{N} G(\boldsymbol{x} - \boldsymbol{x}_i)\boldsymbol{F}_i. \tag{20}$$

The above approximation assumes a coarse-grid EE simulation where the particle size is much smaller than the filter width [38]. From the above definition it is clear that the Eulerian force at a point $x$ represents the weighted average of force on many particles that are in the neighborhood of the point (the extent of the neighborhood is defined by the length scale of the filter function).

Due to the nonlinear dependence of normalized force $\Phi^L$ on $\mathrm{Re}_{@i}$ and $\phi_{@i}$, the average force obtained by averaging over all the particles within the neighborhood of a point $x$ does not depend only on the average Reynolds number and the average volume fraction. Additional knowledge of how $\mathrm{Re}_{@i}$ and $\phi_{@i}$ vary from particle to particle within the averaging volume is necessary in order to properly evaluate the average force.

The added challenge of modeling $\Phi^E$ can now be discussed in relation to the parametrization of the EL counterpart. In going from the Lagrangian modeling of force of an individual particle to the Eulerian modeling of the average force, the effect of the following three different fluctuations must be additionally considered. (i) The Eulerian particle velocity $\boldsymbol{v}(\boldsymbol{x},t)$ accounts for only the average motion of the particles, but the velocity of individual particles in the neighborhood of the point $x$ substantially varies from the average value. (ii) The velocity $\boldsymbol{u}(\boldsymbol{x},t)$ accounts only for the macroscale undisturbed fluid velocity. The actual undisturbed fluid velocity of individual particles in the neighborhood of the point $x$ varies substantially from the average value due to the perturbing effect of the neighboring particles. (iii) The particle volume-fraction field $\phi(\boldsymbol{x},t)$ provides an adequate measure only in the limit where the microstructural distribution is homogeneous and isotropic. In many applications, the distribution of particles can locally be anisotropic and inhomogeneous [16].

Therefore, it is not sufficient to parametrize $\Phi^E$ only in terms of $\mathrm{Re}_{\mathrm{mac}}(\boldsymbol{x},t)$ and $\phi(\boldsymbol{x},t)$. The following additional information is needed.

(a) The nature of particle-to-particle variation in particle velocity must be characterized (i.e., whether the distribution of particle velocity in the neighborhood of the point $x$ is Gaussian log-normal). The magnitude of subgrid particle-velocity variation is characterized in terms of the particle-velocity fluctuation Reynolds number

$$\mathrm{Re}_{Tpx}(\boldsymbol{x},t) = \frac{d v_{\mathrm{rms},x}}{\nu}, \quad \mathrm{Re}_{Tpy}(\boldsymbol{x},t) = \frac{d v_{\mathrm{rms},y}}{\nu}, \quad \mathrm{Re}_{Tpz}(\boldsymbol{x},t) = \frac{d v_{\mathrm{rms},z}}{\nu}, \tag{21}$$

where $v_{\mathrm{rms},x}$, $v_{\mathrm{rms},y}$, and $v_{\mathrm{rms},z}$ are the rms particle-velocity variation. The rms variation in particle velocity along the streamwise ($x$) and transverse ($y$ and $z$) directions can be formally defined as

$$v_{\mathrm{rms},x}^2(\boldsymbol{x},t) = \frac{1}{\phi(\boldsymbol{u},t)} \int_\Omega G(\boldsymbol{x}-\boldsymbol{x}')I_p(\boldsymbol{x}',t)\{[\boldsymbol{v}_{pr}(\boldsymbol{x}',t) - \boldsymbol{v}(\boldsymbol{x},t)] \cdot \boldsymbol{e}_x\}^2 dV,$$

$$v_{\mathrm{rms},y}^2(\boldsymbol{x},t) = \frac{1}{\phi(\boldsymbol{u},t)} \int_\Omega G(\boldsymbol{x}-\boldsymbol{x}')I_p(\boldsymbol{x}',t)\{[\boldsymbol{v}_{pr}(\boldsymbol{x}',t) - \boldsymbol{v}(\boldsymbol{x},t)] \cdot \boldsymbol{e}_y\}^2 dV,$$

$$(22)$$

with a similar definition along the $z$ direction. In granular mechanics, collision-modulated particle-velocity fluctuation is often taken to be isotropic, which leads to the further assumption $\mathrm{Re}_{Tpx} = \mathrm{Re}_{Tpy} = \mathrm{Re}_{Tpz}$. Here we make the assumption that the particle-velocity fluctuation statistics are axisymmetric about the direction of mean relative velocity $\boldsymbol{u}(\boldsymbol{x},t) - \boldsymbol{v}(\boldsymbol{x},t)$, which is taken to be along the $x$ direction. As a result of axisymmetry, $\mathrm{Re}_{Tpy} = \mathrm{Re}_{Tpz}$.

(b) The nature of particle-to-particle variation in the undisturbed fluid velocity evaluated at the particle must be characterized. Its magnitude can be quantified in terms of the undisturbed fluid-velocity fluctuation Reynolds number

$$\mathrm{Re}_{Tfx}(\boldsymbol{x},t) = \frac{du_{\mathrm{rms},x}}{\nu}, \quad \mathrm{Re}_{Tfy}(\boldsymbol{x},t) = \frac{du_{\mathrm{rms},y}}{\nu}, \quad \mathrm{Re}_{Tfz}(\boldsymbol{x},t) = \frac{du_{\mathrm{rms},z}}{\nu}, \qquad (23)$$

where $u_{\mathrm{rms},x}$, $u_{\mathrm{rms},y}$, and $u_{\mathrm{rms},z}$ are the rms undisturbed fluid-velocity variation.

(c) The nature of particle-to-particle variation in the particle volume fraction must be characterized along with its magnitude quantified in terms of the rms of the volume-fraction fluctuation $\phi_{\mathrm{rms}}(\boldsymbol{x},t)$.

(d) Correlation between particle and undisturbed fluid-velocity variation is also of importance (as will be seen in Sec. IV) and can be measured in nondimensional terms as

$$\mathrm{Re}_{Tfpx}(\boldsymbol{x},t) = \frac{dC_x^{1/2}}{\nu}, \quad \mathrm{Re}_{Tfpy}(\boldsymbol{x},t) = \frac{dC_y^{1/2}}{\nu}, \quad \mathrm{Re}_{Tfpz}(\boldsymbol{x},t) = \frac{dC_z^{1/2}}{\nu}, \qquad (24)$$

where $C_x$ is the correlation between the $x$ component of the particle-velocity variation with the $x$ component of the corresponding undisturbed fluid-velocity variation from the average value. The definitions of $C_y$ and $C_z$ are similar.

## III. HOMOGENEOUS DISTRIBUTION OF STATIONARY PARTICLES

We begin with the simplest scenario of a random distribution of stationary particles in a large triply periodic box, inside which the spatial locations of the particles have been chosen with uniform probability. A uniform mean pressure gradient $(\nabla p)_0$ is applied along the mean flow direction (taken to be the $x$ axis), which results in a spatially varying flow around the stationary particles. We consider a box filter of size $\mathscr{L}$, the same as the triply periodic box, so that the macroscale quantities are spatially homogeneous. Let $\mathrm{Re}_{\mathrm{mac}} = \mathrm{Re}_0 = U_0 d/\nu$ be the macroscale Reynolds number, where $U_0$ is the uniform macroscale velocity along the $x$ direction. The problem is characterized by two parameters: the macroscale Reynolds number $\mathrm{Re}_0$ and the uniform particle volume fraction $\phi_0$. This scenario has been considered in several recent particle-resolved simulations [2,3,6,7,9,10,14,39,40].

Since the particles are stationary, there is no particle-velocity variation. Thus, this configuration corresponds to the limit $\mathrm{Re}_{Tpx} = \mathrm{Re}_{Tpx} = \mathrm{Re}_{Tpx} = 0$. Furthermore, due to the uniform random distribution of particles and the choice of box filter, the macroscale volume fraction is uniform and $\phi' = 0$. Thus, the only particle-to-particle variation is in the undisturbed fluid velocity at the particles. Here we restrict attention to modest values of the mean Reynolds number, so the flow is steady. In the present problem, the macroscale undisturbed fluid velocity of all the particles is the same as $U_0$. As illustrated in Fig. 1, the microscale undisturbed velocity of each particle depends on the precise arrangement of its neighbors and therefore can be substantially different from one particle to another. For example, the microscale undisturbed velocity of a particle which happens to

TABLE I. Different volume fraction and Reynolds-number ranges considered.

| Case | Volume fraction | Box size $L/d$ | No. of particles | Realizations | $Re_0$ |
|---|---|---|---|---|---|
| 1 | 0.11 | 30.57 | 1000 | 6 | 0–110 |
| 2 | 0.21 | 24.64 | 1000 | 6 | 0–160 |
| 3 | 0.45 | 19.11 | 1000 | 6 | 0–160 |

lie in the immediate wake of other upstream particles will be substantially negative, while that of a particle that happens to be located in the high-speed flow channel will be substantially positive.

Three different configurations at volume fractions of 11%, 21%, and 45% are considered. Each system contains a triply periodic box within which 1000 particles are randomly distributed with uniform probability. The size of the triply periodic box is chosen to yield the appropriate mean volume fraction (the details are given in Table I). The mean interparticle distances for the three volume fractions are 2.09, 1.68, and 1.30 particle diameters, respectively. Each configuration is repeated with six realizations and the results to be presented are averaged over all the particles in all the realizations. For each volume fraction, a range of Reynolds numbers between 0 and 160 is considered. The choice of volume fraction and the range of $Re_0$ are based on available superposable wake maps.

The distribution of $u_{\text{mic@i}}$ both along the flow direction and along the transverse direction is of interest here. As presented in (17), the microscale contribution to the undisturbed flow velocity is approximated by a superposition of surface averages of superposable wakes of nearby neighbors to define $u_{\text{mic@i,x}} = \sum_{j=1}^{\prime N} \overline{(u_{sw,x})_j}^{S_i}$, with similar definitions that apply for the $y$ and $z$ components. Here $(u_{sw,x})_j$ represents the streamwise component of the $j$th neighbor's superposable wake, whose average over the surface of the $i$th particle is denoted by the overbar and the superscript $S_i$. It has been observed in [17] that the axisymmetric maps $\overline{(u_{sw,x})}^S$ and $\overline{(u_{sw,y})}^S$ decay rapidly and are nonzero only over a cylinder of radius $4.3d$ whose axial length extends from $-4.2d$ to $6.5d$ along the flow direction. Thus, for each particle the contribution to the superposition of surface averages of superposable wakes is limited to only those neighbors that are within this cylinder of influence. Also, superposable wakes have been properly defined in order to render the microscale undisturbed flow a true perturbation quantity and therefore not alter the undisturbed flow averaged over all the particles, i.e., it is ensured that the mean values

$$\langle u_{\text{mic@i,x}} \rangle = \frac{1}{N} \sum_{i=1}^{N} u_{\text{mic@i,x}} = 0, \quad \langle u_{\text{mic@i,y}} \rangle = \langle u_{\text{mic@i,z}} \rangle = 0. \tag{25}$$

Thus, the microscale undisturbed flow of each particle can be considered as fluctuation away from the mean macroscale undisturbed velocity, which in the present problem equals $U_0$ along the $x$ axis.

Normalized histograms of $u_{\text{mic@i,x}}/U_0$ and $u_{\text{mic@i,y}}/U_0$ are shown in Fig. 2 for three different combinations of $Re_0$ and $\phi_0$. The histogram of the $z$ component is the same as that of the $y$ component. Also plotted as red lines in all the figures are the best-fitting probability density functions (PDFs) of the histogram. It can be observed that the distribution of the transverse component of the undisturbed velocity fluctuation at the particles follows a Gaussian PDF for all combinations of the macroscale Reynolds number and volume fraction. The width of the distribution appears to increase with $Re_0$ and $\phi_0$. In the case of the streamwise component, the distribution follows a shifted $\Gamma$ distribution at lower volume fraction and tends to become a Gaussian PDF at higher volume fraction.

The asymmetric nature of the distribution at low volume fraction can be explained in terms of the fore-aft asymmetry of the wake at finite Reynolds numbers. The strong negative-velocity perturbation in the wake and in the front stagnation point region of a particle is compensated by a very broad region of weak positive-velocity perturbation along its equatorial sides. This feature
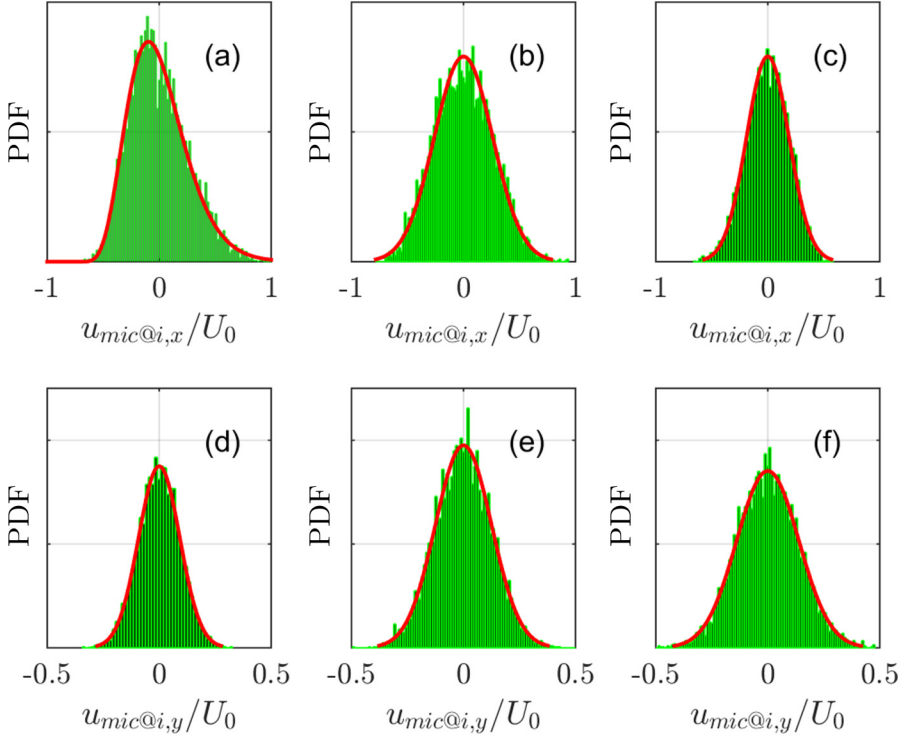
FIG. 2. Normalized histograms of (a)–(c) the streamwise component of the surface averaged undisturbed velocity fluctuation at the particles and (d)–(f) the transverse component of the undisturbed velocity fluctuation at the particles for (a) and (d) $Re_0 = 100$ and $\phi_0 = 0.11$, (b) and (e) $Re_0 = 60$ and $\phi_0 = 0.21$, and (c) and (f) $Re_0 = 30$ and $\phi_0 = 0.45$. In all the plots the red curve shows the best-fitting analytical distribution. In (a) the best fit is a $\Gamma$ distribution, while in all others a Gaussian fit is shown.

of velocity perturbation is responsible for the positive skewness of the $u_{\text{mic@i,x}}$ distribution. With increasing volume fraction, it was reported in [33] that the fore-aft asymmetry of the superposable wake decreases, since the individual particle wakes are increasingly broken up by the neighboring particles. This is reflected in the more symmetric nature of $u_{\text{mic@i,x}}$ distribution at the higher volume fraction. Figure 3 shows scatter plots of the normalized $x$ component plotted against the normalized $y$ component for the three combinations of $Re_0$ and $\phi_0$ shown in Fig. 2. From the plots it is clear that there is no systematic correlation between the streamwise and transverse components. This is to be
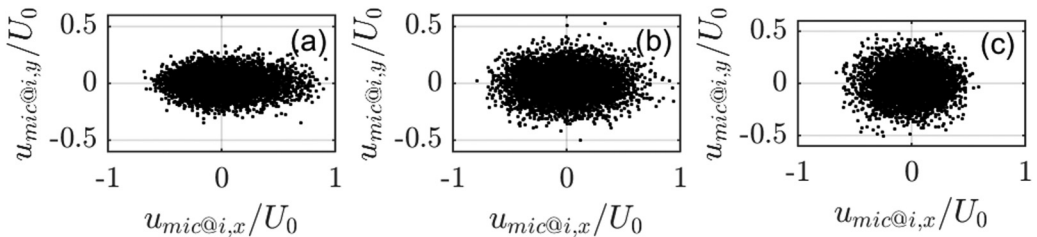


FIG. 3. Scatter plot of streamwise component of the surface averaged undisturbed velocity fluctuation versus the transverse component for all the particles within the system for (a) $Re_0 = 100$ and $\phi_0 = 0.11$, (b) $Re_0 = 60$ and $\phi_0 = 0.21$, and (c) $Re_0 = 30$ and $\phi_0 = 0.45$.
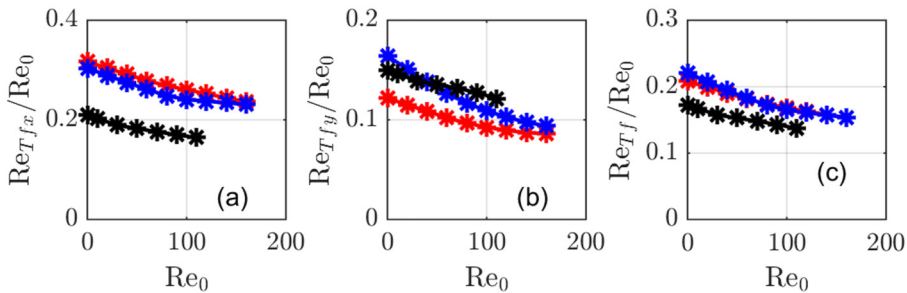
FIG. 4. Plot of rms normalized (a) streamwise, (b) transverse, and (c) total particle-to-particle-velocity fluctuation. The results are shown for a range of macroscale Reynolds number. Three different volume fractions are shown: $\phi_0 = 11\%$ (red), $\phi_0 = 21\%$ (blue), and $\phi_0 = 45\%$ (black).

expected due to both the uniform random distribution of particles and the symmetries or periodicity of the problem.

Hitherto it has not been easy to estimate the level of fluid-velocity fluctuation seen by the particles in a multiphase flow. The use of a superposable wake with the pairwise interaction approximation of the PIEP model has given us an opportunity to obtain such an estimate. From Fig. 2 it is clear that the level of particle-to-particle variation in the undisturbed fluid velocity at the particle is substantial. In the case of the streamwise component, the fluctuation can be as large as 100%, which indicates that, given a macroscale Reynolds number of $\mathrm{Re}_0$, the Reynolds number of an individual particle could be as low as zero or can be as high as twice the macroscale value. Furthermore, it is important to note that each particle within the array is subjected to a substantial local fluid velocity that is not aligned in the direction of the macroscale flow. The transverse velocity can be as high as 40%. The resulting particle-to-particle transverse force variation will likely play an important role in transverse diffusion and dispersion.

It must however be noted that the distributions of undisturbed fluid velocities shown in Fig. 2 are perhaps sightly underestimated. It has been shown in [33] that the subgrid velocity fluctuation evaluated using the superposition of superposable wakes slightly underestimates the actual velocity fluctuation computed in a particle-resolved simulation. The effect of this underestimation may however be mollified by the fact that the undisturbed velocity has been averaged over its surface. Furthermore, the superposable wakes account for only the pseudoturbulent component. Though not important in the present demonstration, in other applications subgrid velocity fluctuations may also include unresolved turbulence.

### A. Fluid-velocity-induced Reynolds-number fluctuation

The microscale undisturbed velocity of all $N$ particles within the system, computed via the surface average in Eq. (12), can then be used to calculate the rms Reynolds-number fluctuation in the following way:

$$\mathrm{Re}_{Tfx} = \frac{d}{\nu} \sqrt{\frac{1}{N} \sum_{i=1}^{N} [u_{\mathrm{mic@i,x}}]^2}. \qquad (26)$$

In the above, we have taken the mean value of $u_{\mathrm{mic@i,x}}$ to be zero. If similarly defined, due to the axisymmetric nature of the statistics about the mean flow direction, we expect $\mathrm{Re}_{Tfy} = \mathrm{Re}_{Tfz}$. Figure 4 shows plots of $\mathrm{Re}_{Tfx}/\mathrm{Re}_0$, $\mathrm{Re}_{Tfy}/\mathrm{Re}_0$, and $\mathrm{Re}_{Tf}/\mathrm{Re}_0$ for a range of macroscale Reynolds numbers for three different volume fractions. Figure 4(a) shows that particle-to-particle variation in the normalized streamwise component of undisturbed velocity decreases with both the macroscale Reynolds number and volume fraction. It should be pointed out that in the zero-

volume-fraction limit of nearly isolated particles, each particle is uninfluenced by its neighbors and thus $\text{Re}_{Tfx}$, $\text{Re}_{Tfy}$, $\text{Re}_{Tfz} \to 0$. It is thus interesting to observe that the normalized streamwise velocity variation rapidly increases in the modest volume fraction range of 0%–11%. A decrease in $\text{Re}_{Tfx}/\text{Re}_0$ with a further increase in volume fraction is not entirely surprising, since as observed in [33], due to the collective effect of the increasing number of close-by neighbors, the extent of each particle's superposable wake is greatly reduced with increasing volume fraction. Unfortunately, with the limited availability of particle-resolved simulations it is not possible to identify at what macroscale volume fraction the rms fluctuation reaches its maximum value. It is nevertheless clear that the level of particle-to-particle variation is substantial.

In Fig. 4(b) the behavior of the normalized transverse velocity fluctuation is somewhat more complex. At higher $\text{Re}_0$, $\text{Re}_{Tfy}/\text{Re}_0$ tends to increase with increasing volume fraction. At lower $\text{Re}_0$, there appears to be a nonmonotonic trend, with the level of transverse velocity fluctuation first increasing with increasing volume fraction, reaching a maximum, and then decreasing with a further increase in $\phi_0$. As with the streamwise component, the transverse component also decreases with increasing Reynolds number. The rms of the undisturbed fluid-velocity fluctuation, which is the fluid analog of granular temperature, can be defined as

$$\text{Re}_{Tf} = [\tfrac{1}{3}(\text{Re}_{Tfx}^2 + 2\,\text{Re}_{Tfy}^2)]^{1/2}. \tag{27}$$

Variation of $\text{Re}_{Tf}/\text{Re}_0$ is presented in Fig. 4(c). From the figure it appears that with $\phi_0$ increasing from 0 to ∼10% the fluctuation Reynolds number increases, reaches a peak, remains invariant to further increase in volume fraction to about 21%, and then decreases with a further increase in volume fraction.

### B. Eulerian force model (stationary particles)

In this section we use our understanding of the particle-to-particle variation in undisturbed flow velocity to examine the existing drag models and advance alternative models as appropriate. Again we restrict attention to a uniform macroscale flow through a uniform distribution of stationary particles. Thus the problem is statistically homogeneous and is characterized by the two macroscale parameters $\text{Re}_0$ and $\phi_0$, which remain the same for all particles. First, we consider the average streamwise drag on the particles; this is the information that is required in a typical Euler-Euler simulation. In the present context, following (19), the average drag after normalization can be expressed as

$$\Phi_0^E = \frac{\frac{1}{N}\sum_{i=1}^{N} \boldsymbol{F}_i \cdot \boldsymbol{e}_x}{3\pi \mu d U_0}, \tag{28}$$

where $\boldsymbol{F}_i \cdot \boldsymbol{e}_x$ corresponds to the streamwise component of the force on the $i$th particle and the average is over all the particles within the homogeneous system. We now clarify the notation: In $\Phi_0^E$, the subscript 0 corresponds to stationary, homogeneous, and isotropic distribution of particles. As a result of these restrictions, $\Phi_0^E$ will depend only on the two macroscale parameters $\text{Re}_0$ and $\phi_0$. When evaluated in this manner, the resulting $\Phi_0^E$ will be inappropriate under conditions where the distribution of particles is inhomogeneous and anisotropic and when the particles are allowed to freely move, which will introduce substantial particle-velocity variation.

Several models of $\Phi_0^E(\text{Re}_0, \phi_0)$ have been proposed in recent years, mainly based on results from a large collection of particle-resolved simulations [2,3,6,7,9,10]. We draw attention to the fact that the above list does not include the classic drag correlations [4,5,8], since these correlations are based on systems where the particles are allowed to move freely. As pointed out in [31], the latter correlations must therefore account for the added effects of particle velocity and local volume fraction variation. As an example, we present the average drag correlation of [7] in normalized form

as

$$\Phi_0^E(\mathrm{Re}_0, \phi_0) = \left[ \frac{1 + 0.15\,\mathrm{Re}_0^{0.687}}{(1-\phi_0)^2} + \underbrace{\frac{5.81\phi_0}{(1-\phi_0)^2} + \frac{0.48\phi_0^{1/3}}{(1-\phi_0)^3}}_{f_1(\phi_0)} + \underbrace{\phi_0^3(1-\phi_0)\mathrm{Re}_0\left(0.95 + \frac{0.61\phi_0^3}{(1-\phi_0)^2}\right)}_{f_2(\mathrm{Re}_0,\phi_0)} \right].$$

(29)

The above correlation and other similar ones proposed in [2,3,6,9,10] differ somewhat from each other. Though differences in the numerical methodology (finite difference vs lattice Boltzmann), degree of resolution, and the manner in which particles are randomly distributed are expected to contribute, a complete explanation of differences is still lacking. Nevertheless, the discussion to follow using the drag correlation of [7] can easily be replicated with any other correlation.

Figure 5 shows plots of $\Phi_0^E$ (shown as the blue solid line) calculated using the above correlation as a function of $\mathrm{Re}_0$ for the three different volume fractions of $\phi_0 = 0.11$, 0.21, and 0.45. Also plotted as a black dashed line is the corresponding normalized drag evaluated using the standard drag relation of an isolated particle, i.e., using $(1 + 0.15\,\mathrm{Re}_0^{0.687})$. Since the standard drag law is independent of $\phi$, the black dashed line is the same in all three frames. The large difference between the blue solid line and the black dashed line highlights the profound effect of neighboring particles in substantially increasing the average drag. There are two sources that contribute to this difference. (i) As discussed in the preceding section, the undisturbed fluid velocity varies from particle to particle with the particle's relative velocity being sometimes substantially larger or lower than the average. Since the drag force's dependence on the undisturbed fluid velocity is nonlinear, the true average force is larger than that computed based on the average relative velocity. (ii) For the same undisturbed fluid velocity, the drag force on a particle in the presence of neighbors is different from that of an isolated particle. The latter effect is due to the fact that the self-perturbation flow of a particle is influenced by the presence of neighbors (as a result of their no-slip and no-penetration boundary conditions).

Since we can compute the undisturbed flow of each particle within the random distribution using the superposition of nearby neighbor's superposable wakes, the two effects can be separated as follows. The first effect of particle-to-particle variation in the undisturbed flow can be taken into account by computing the drag on each particle using its undisturbed fluid velocity in the standard drag law and then averaging over all the particles to obtain

$$\frac{\frac{1}{N}\sum_{i=1}^N (\boldsymbol{u}_{@i} \cdot \boldsymbol{e}_x)(1.0 + 0.15\,\mathrm{Re}_{@i}^{0.687})}{U_0}.$$

(30)

By assuming the drag on each particle to be given by the standard drag law of an isolated particle, the above ignores the second effect of the influence of neighboring particles on the self-perturbation flow and only accounts for the variation in the undisturbed fluid velocity. Plots of normalized average drag computed as the summation given in (30) are shown in Fig. 5 as the red dashed lines. The undisturbed fluid-velocity variation contributes only modestly to the increase in the average drag force; this influence is larger at lower volume fraction and progressively decreases with increasing volume fraction.

The summation given in (30) can be carried out after expanding $\boldsymbol{u}_{@i}$ about the mean velocity $U_0\boldsymbol{e}_x$ (see Appendix D) to obtain

$$\underbrace{1 + 0.15\,\mathrm{Re}_0^{0.687}}_{\text{standard drag}} + \underbrace{\frac{0.15 \times 0.687}{2\,\mathrm{Re}_0^{1.313}}(1.687\,\mathrm{Re}_{Tfx}^2 + 2.0\,\mathrm{Re}_{Tfy}^2)}_{\text{leading effect of undisturbed flow variation}} + \cdots,$$

(31)

where the ellipsis denotes higher-order terms. The above expression provides an excellent approximation and explains the contribution of the particle-to-particle variation in the undisturbed flow velocity. The variance of streamwise velocity fluctuation measured in terms of $\mathrm{Re}_{Tfx}^2$ contributes
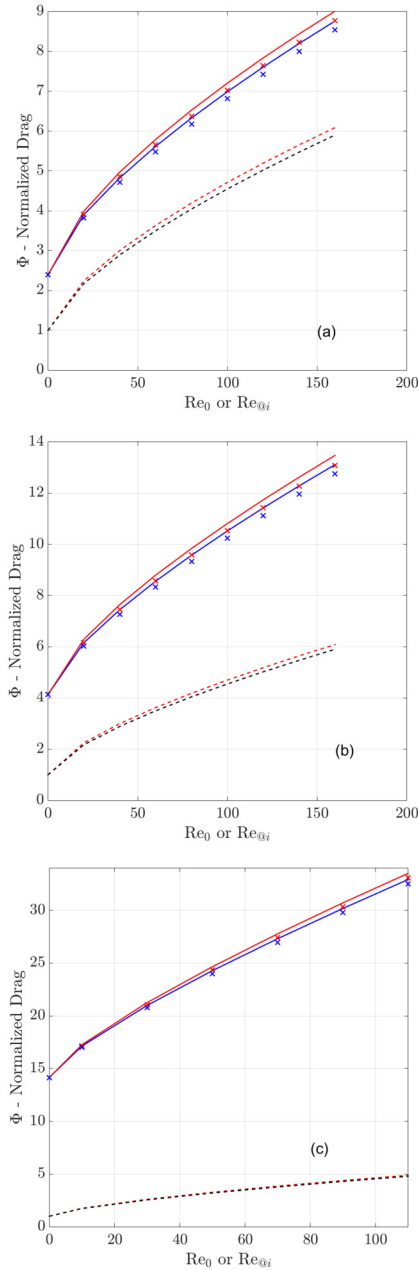
FIG. 5. Comparison of various evaluations of normalized drag plotted as a function of Reynolds number for (a) $\phi_0 = 0.11$, (b) $\phi_0 = 0.21$, and (c) $\phi_0 = 0.45$. The black dashed line shows the standard drag evaluated as a function of macroscale Reynolds number $Re_0$, the red dashed line shows the standard drag evaluated at each particle based on its Reynolds number $Re_{@i}$ and then averaged, the blue solid line shows the Eulerian normalized average drag calculated using (29) as a function of the macroscale Reynolds number $Re_0$, blue crosses show the Lagrangian normalized drag calculated using (33) as a function of the macroscale Reynolds number $Re_0$, the red solid line shows the Eulerian normalized drag (29) inappropriately calculated at each particle based on its Reynolds number $Re_{@i}$ and then averaged, and the red crosses show the Lagrangian normalized drag (33) properly calculated at each particle based on its Reynolds number $Re_{@i}$ and then averaged. Note that the red crosses are in excellent agreement with the blue solid line.

68.7% more than the variance of each of the transverse velocity fluctuation. Furthermore, as can be seen in Fig. 4, $\text{Re}_{Tfx}^2$ is typically much larger than $\text{Re}_{Tfy}^2$. Nevertheless, at the level of undisturbed velocity fluctuation presented in Fig. 4, the increase in average drag is modest (i.e., the difference between the black and the red dashed lines is small); however, Eq. (31) indicates that with a further increase in the fluctuation Reynolds number, for example, through particle-velocity variation when particles are allowed to move, the increase in average drag can be higher. In any case, in Fig. 5 the major contributor to the large difference between $\Phi_0^E$ (blue solid line) and the standard drag (black dashed line) is the influence of neighboring particles on the self-induced perturbation flow.

### C. Lagrangian force model (stationary particles)

An important point of the earlier discussion is that when a nonlinear drag correlation, such as the standard drag law, is applied for each individual particle and then averaged over all the particles, the resulting average will be higher than when the correlation is applied to the average particle motion. This has an important implication in the application of the Eulerian normalized average drag correlation $\Phi_0^E$, such as the one given in (29).

The difference between an EL-mac simulation of flow over a stationary random distribution of particles and the corresponding EE simulation is small and therefore $\Phi_0^E$ can be applied for each particle of the EL-mac simulation. The resulting force variation among the particles in a neighborhood will be quite small. It is however inappropriate to use $\Phi_0^E$ in the evaluation of force on individual particles in an EL-mic simulation. This is because drag on individual particles computed this way will vary within a neighborhood, which when averaged over all the particles will be larger, and exceed the average drag correlation $\Phi_0^E$.

We define $\Phi_0^L$ as the consistent Lagrangian normalized force correlation (for stationary particles as indicated by the subscript 0), which when applied to and averaged over all the particles will correctly yield the appropriate Eulerian normalized force correlation $\Phi_0^E$. This force consistency relation can be mathematically expressed as

$$U_0 \Phi_0^E(\text{Re}_0, \phi_0) = \frac{1}{N} \sum_{i=1}^{N} (\boldsymbol{u}_{@i} \cdot \boldsymbol{e}_x) \Phi_0^L(\text{Re}_{@i}, \phi_0), \tag{32}$$

where we have canceled the common factor $3\pi \mu d$ on both sides. In the present context of a uniform macroscale flow in a periodic box with a random distribution of stationary particles, the normalized average force $\Phi_0^E$ is a function of the macroscale Reynolds number $\text{Re}_0$ and volume fraction $\phi_0$. On the other hand, the Lagrangian normalized force $\Phi_0^L$ is a function of the Reynolds number of the individual particle, whose undisturbed fluid velocity depends on the relative location of its neighbors, while the volume fraction remains the same for all particles. From the above, it is clear that in general $\Phi_0^E \neq \Phi_0^L$ and the equality applies only in the case when there is no particle-to-particle variation in the undisturbed fluid velocity or in the Stokes limit of low Reynolds number when the normalized force is linear in relative velocity.

The above consistency relation can be viewed as an inverse problem of finding the consistent Lagrangian normalized force correlation $\Phi_0^L$, which when averaged as given in the above equation will yield the desired Eulerian normalized drag $\Phi_0^E$, such as the one given in (29). By a Taylor series expansion of the right-hand side of (32) about the macroscale Reynolds number $\text{Re}_0$ and following the steps of Appendix D it can be readily seen that $\Phi_0^L$ will be lower than $\Phi_0^E$. An approximate curve fit of the inverse problem yields the expression

$$\Phi_0^L(\text{Re}_{@i}, \phi_0) = \left[ \frac{1 + 0.15\,\text{Re}_{@i}^{0.687} f_3(\text{Re}_{@i}, \phi_0)}{(1 - \phi_0)^2} + f_1(\phi_0) + f_2(\text{Re}_{@i}, \phi_0) \right], \tag{33}$$

where the functions $f_1(\phi_0)$ and $f_2(\text{Re}_0, \phi_0)$ are the same as in (29) and

$$f_3(\text{Re}_{@i}, \phi_0) = 1 - 1.5\phi_0^{1.217} e^{-5.44\phi_0} (1.0 - 0.0051\,\text{Re}_{@i} + 1.71 \times 10^{-5}\text{Re}_{@i}^2). \tag{34}$$

The above is the Lagrangian counterpart of the Eulerian drag correlation given in (29). Both apply only in the limit when the particles are not moving with respect to each other, i.e., when the particles are stationary relative to each other.

Plots of $\Phi_0^L$ as a function of $\mathrm{Re}_{@i}$ for the three different volume fractions are also shown in Fig. 5 as the blue crosses. As expected, $\Phi_0^L$ is lower than $\Phi_0^E$, which is the blue solid line. The difference, though noticeable, is not very large and decreases with increasing volume fraction. The small difference is again due to the limited range of particle-to-particle variation in the undisturbed fluid velocity (i.e., due to modest values $\mathrm{Re}_{Tfx}$ and $\mathrm{Re}_{Tfy}$ as given in Fig. 4). As a check, an average over all the particles was performed after calculating the normalized drag force on each particle using $\Phi_0^L$. This average is also shown in Fig. 5 as the red crosses. The agreement between the red crosses and $\Phi_0^E$ (blue solid line) is quite good.

Clearly the Lagrangian correlation given in (33) and (34) is just one possible fit of the force consistency relation. Here the drag on the particle has been parametrized only in terms of the surface-averaged undisturbed fluid velocity, through the dependence on $\mathrm{Re}_{@i}$. While $\Phi_0^L$ defined this way matches the Eulerian counterpart $\Phi_0^E$ upon averaging, there is no guarantee that force on individual particles will best match their PR DNS values. Nor will higher-order statistics such as the rms of particle-to-particle force variation match those of PR DNS. To achieve a more accurate deterministic prediction, the force expression must additionally depend on the volume average of the undisturbed stress divergence and on the volume-averaged vorticity. This will allow accurate accounting of other contributions from the undisturbed flow force, added-mass force, vorticity-induced lift force, etc. (see PIEP force modeling presented in [11,12,37]). Here we proceed with (33) and (34) for their simplicity. Nevertheless, this correlation is of fundamental importance, since the difference between the standard drag of an isolated particle (black solid line) and $\Phi_0^L$ (blue crosses) embodies the effect of neighbors in increasing the drag on an individual particle within a random stationary array. Only upon further averaging over many particles do we arrive at $\Phi_0^E$ (blue solid line).

The difference between $\Phi_0^L$ and $\Phi_0^E$ has been accounted for through the function $f_3$. In the dilute limit of $\phi_0 \to 0$, the function $f_3 \to 1$, since each particle remains unaffected by the presence of very distant neighbors and the undisturbed flow has no microscale component. In the Stokes limit of $\mathrm{Re} \to 0$, the influence of $f_3$ vanishes. Thus, in both these limits $\Phi_0^L = \Phi_0^E$. Eulerian drag correlations, such as those given in (29), have been used in EL-mic simulations. Such application of the average drag correlation to individual particles will result in a slight overestimation of the overall drag force. This effect is shown in Fig. 5, where the average

$$\frac{1}{N} \sum_{i=1}^{N} \frac{\boldsymbol{u}_{@i} \cdot \boldsymbol{e}_x}{U_0} \Phi_{H,S}^E(\mathrm{Re}_{@i}, \phi_0) \tag{35}$$

is plotted as a red solid line. In this case, the Eulerian average drag correlation of (29) has been inappropriately applied to each particle and then averaged to yield the red solid line. As expected, this contributes to an increase in the average drag above the expected value of $\Phi_0^E$.

The difference between $\Phi_0^E$ and $\Phi_0^L$ (i.e., the difference between the blue solid line and the blue crosses in Fig. 5) is due to particle-to-particle variation in $\mathrm{Re}_{@i}$, which in turn is due to variation in the streamwise and transverse components of the undisturbed fluid velocity at the particles. We now separate the contribution of the streamwise and the transverse undisturbed fluid-velocity variation. Such separation will be exploited in the next section where we proceed to extend the Eulerian drag correlation to nonstationary problems. Towards this goal we expand in a Taylor series $\Phi_0^L(\mathrm{Re}_{@i}, \phi_0)$ about the macroscale state $(\mathrm{Re}_0, \phi_0)$ and substitute the expansion into the right-hand side of (32). Rewriting the ratio $(\boldsymbol{u}_{@i} \cdot \boldsymbol{e}_x)/U_0$ as $\mathrm{Re}_{@ix}/\mathrm{Re}_0$, we follow the steps of Appendix D to obtain the
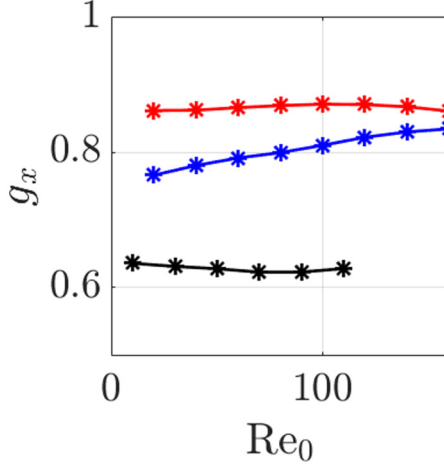
FIG. 6. Plot of fractional contribution to the difference between the Eulerian and Lagrangian normalized drag (i.e., between $\Phi_0^E$ and $\Phi_0^L$) from the particle-to-particle streamwise undisturbed fluid-velocity variation in the case of flow past a uniform random distribution of stationary particles. The three lines correspond to $\phi_0 = 0.11$ (red), $\phi_0 = 0.21$ (blue), and $\phi_0 = 0.45$ (black).

relation

$$\Phi_0^E(\text{Re}_0, \phi_0) = \Phi_0^L(\text{Re}_0, \phi_0) + \left[ \frac{1}{2} \frac{\partial^2 \hat{\Phi}_0^L}{\partial \text{Re}_{@ix}^2} \right]_0 \left( \frac{1}{N} \sum_{i=1}^N (\text{Re}_{@ix} - \text{Re}_0)^2 \right)$$

$$+ \left[ \frac{\partial^2 \hat{\Phi}_0^L}{\partial \text{Re}_{@iy}^2} \right]_0 \left( \frac{1}{N} \sum_{i=1}^N \text{Re}_{@iy}^2 \right)$$

$$= \Phi_0^L(\text{Re}_0, \phi_0) + \left[ \frac{1}{2} \frac{\partial^2 \hat{\Phi}_0^L}{\partial \text{Re}_{@ix}^2} \right]_0 \text{Re}_{Tfx0}^2 + \left[ \frac{\partial^2 \hat{\Phi}_0^L}{\partial \text{Re}_{@iy}^2} \right]_0 \text{Re}_{Tfy0}^2, \tag{36}$$

where $\hat{\Phi}$ is introduced in Appendix D. At small Re an exact integration over the Maxwellian distribution can be performed as discussed in [41]. In obtaining the second equality we have used the Reynolds-number definitions of streamwise and transverse undisturbed fluid-velocity fluctuations at the particles given in (26). We now define the fractional contribution to the difference between the Eulerian and the Lagrangian normalized drag from the streamwise component to be

$$g_x(\text{Re}_0, \phi_0) = \frac{\left[ \frac{1}{2} \frac{\partial^2 \hat{\Phi}_0^L}{\partial \text{Re}_{@ix}^2} \right]_0 \text{Re}_{Tfx0}^2}{\Phi_0^E(\text{Re}_0, \phi_0) - \Phi_0^L(\text{Re}_0, \phi_0)}. \tag{37}$$

A plot of $g_x$ as a function of $\text{Re}_0$ for three different values of $\phi_0$ is shown in Fig. 6. It can be seen that except at the intermediate volume fraction, $g_x$ is nearly independent of $\text{Re}_0$. At lower volume fraction nearly 86% of the increase comes from the particle-to-particle streamwise undisturbed fluid-velocity variation and the contribution decreases with increasing volume fraction. At $\phi_0 = 0.45$, the streamwise undisturbed fluid-velocity variation contributes 63%. A simple curve fit, assuming $g_x$ to be approximately independent of $\text{Re}_0$, is given by

$$g_x = 0.927 - 0.513\phi_0 - 0.337\phi_0^2. \tag{38}$$

By definition, the fractional contribution along the transverse directions is given by $g_{y,z} = 1 - g_x$.

## IV. HOMOGENEOUS DISTRIBUTION OF NONSTATIONARY PARTICLES

This section considers particles in motion and our goals are to identity (i) an appropriate Lagrangian model of the normalized drag that can be applied to each particle within the system and (ii) an Eulerian model of the normalized average drag that is appropriate for a group of particles that lie within the averaging volume. Two additional mechanisms make this problem more complicated than the stationary particles considered in the preceding section. When particles are allowed to move freely, the particle-to particle variation in relative velocity changes, since this variation arises not only from the undisturbed fluid velocity, but also from the particle velocity [31,41,42]. In granular flows, it is well understood that interparticle collisions lead to large departures in the motion of individual particles away from the mean particle velocity. Even in the absence of direct collisions between particles, the fluid-mediated interaction between the particles will contribute to particle-velocity fluctuation away from the mean.

Another important effect of particle motion is that homogeneity of the particle distribution and the uniformity of the particle volume fraction cannot be guaranteed. In addition, the microstructure of the particle distribution as quantified by statistics such as the radial distribution function may not be isotropic. The variation in particle velocity, the departure from the uniform distribution of particles, and the nonisotropic microstructure of neighboring particles will all contribute to the determination of particle force at the level of both an individual particle and an average over the averaging volume. In the present work we will restrict attention to only the effect of particle-to-particle variation in particle velocity. We will assume the particle distribution to remain homogeneous and the microstructure to remain isotropic.

### A. EL-mic viewpoint

Here we consider force on an individual particle, when particles are in free motion but under the conditions of a uniform random distribution. The macroscale state of the system must now be characterized by the macroscale Reynolds number $\text{Re}_0$, the local particle volume fraction $\phi_0$, and the granular temperature or the level of particle-velocity fluctuation, quantified by $\text{Re}_{Tpx}$ and $\text{Re}_{Tpy}$.

The particle-velocity variation influences the drag on the $i$th particle in several ways. (i) The deviation of the $i$th particle's velocity from the macroscale value is easy to account for in the Lagrangian framework. Since the velocity of each particle is being tracked, the drag force model can properly account for the particle velocity. (ii) The deviation of the neighbors' velocity from the macroscale value influences its perturbation flow. As a result, the undisturbed flow at the $i$th particle will be influenced by the motion of the neighboring particles. The effect of the neighbors' motion on the undisturbed flow of the $i$th particle can be taken into account with the use of the PIEP model and superposable wakes. (iii) The relative motion of the neighboring particles with respect to the $i$th particle also influences the self-induced perturbation flow of the $i$th particle.

Based on the above considerations, we pursue the following force modeling strategy in the EL-mic framework.

*Step 1*. For each particle calculate its surface-averaged undisturbed fluid velocity as outlined in Eq. (17).

*Step 2*. From the surface-averaged undisturbed fluid velocity and the particle velocity calculate the Reynolds number $\text{Re}_{@i}$ of the particle.

*Step 3*. From $\text{Re}_{@i}$ and $\phi_{@i}$ of the particle evaluate the force on the particle using the Lagrangian drag correlation $\Phi_0^L$.

This three-step process of evaluating the force on each particle is the same as that for the stationary case. However, application of these steps to a nonstationary system involves two fundamental assumptions. First, in the evaluation of the undisturbed fluid velocity, in Eq. (17), the superposable wakes should have been evaluated for the configuration of nonstationary particles; however, such information is not currently available. Therefore, the superposable wakes of the stationary configuration, as obtained in [33], have be used in the nonstationary configuration as

well. Second, the Lagrangian force correlation $\Phi_0^L$ defined in Sec. III C has been developed based on the results of PR simulations of a stationary configuration. Thus, the use of $\Phi_0^L$ in the present context of moving particles is an assumption. In any case, without additional PR simulations of nonstationary particles, the above strategy is the only viable option.

## B. EE viewpoint

Here we consider modeling of the average force that has been averaged over a large number of moving particles but under the conditions of a uniform random distribution. The level of particle-velocity fluctuation measured in terms of $\mathrm{Re}_{Tpx}$ and $\mathrm{Re}_{Tpy}$ will be strongly dependent on the particle Stokes number [31,43,44]. Since the particle Stokes number has been defined as the ratio of the particle-to-fluid timescale, in a turbulent flow, a range of Stokes numbers can be identified for each particle, with the Stokes number based on the integral scales being the smallest and the Stokes number based on Kolmogorov eddies being the largest. Three different regimes can be identified [45,46]. Regime I corresponds to when the Stokes number based on the Kolmogorov scale is much smaller than unity (i.e., $\mathrm{St}_k \ll 1$) and in this regime particles nearly follow the fluid. Regime III is characterized by large particles whose Stokes number based on the integral scale is larger than unity (i.e., $\mathrm{St}_L \gg 1$) and in this regime particles are ballistic and do not respond to turbulent eddies. Then, by definition, in the intermediate regime II there exists a turbulent eddy scale that matches the particle timescale and therefore the regime-II particles are most responsive to flow turbulence. Based on this classification of particle response, we may expect the dependence of $\mathrm{Re}_{Tpx}$ and $\mathrm{Re}_{Tpy}$ on the particle Stokes number to be nonmonotonic and complex.

The force on a particle is dependent on the difference between the undisturbed fluid velocity and the particle velocity. Thus, particle-to-particle variation in force is related to variation in the relative velocity and not just on $\mathrm{Re}_{Tfx}$, $\mathrm{Re}_{Tfy}$, $\mathrm{Re}_{Tpx}$, and $\mathrm{Re}_{Tpy}$. In regime III, where particle motion is uncorrelated with the fluid-velocity fluctuations, the variance of relative velocity variation can be taken to be the sum of the variance of the undisturbed fluid velocity and the variance of the particle-velocity variation. Since the fluid and particle-velocity fluctuations are additive, we expect the Eulerian average to increase substantially over the Lagrangian counterpart. In contrast, in regime I, the particle-velocity fluctuation will be highly correlated with the undisturbed fluid-velocity fluctuation. Therefore, even when these fluctuations are large, force variation within the averaging volume will not be large and the Eulerian average will be nearly the same as the Lagrangian counterpart. This difference in the average force of large- and small-Stokes-number particles has been well illustrated in the work of [31].

In an EE simulation that does not employ additional equations for granular temperature, $\mathrm{Re}_{Tpx}$ and $\mathrm{Re}_{Tpy}$ must be parametrized in terms of local values of $\mathrm{Re}(\boldsymbol{x}, t)$, $\phi(\boldsymbol{x}, t)$, and the Stokes number $\mathrm{St}(\boldsymbol{x}, t)$, which can be chosen to be that based on Kolmogorov eddies. While the first two parameters dictate the level of microscale fluid-velocity fluctuation seen by the particles, the last parameter accounts for the particle's ability to respond to these fluid-velocity fluctuations. Since the particle-to-fluid density ratio $\rho_p/\rho_f$ is an important parameter that dictates the particle Stokes number, the density ratio has also been used for parametrization instead of the Stokes number [31,44].

In this work we will neither attempt to predict $\mathrm{Re}_{Tpx}$ and $\mathrm{Re}_{Tpy}$ as a function of the macroscale parameters nor obtain it from a granular temperature equation. Instead, we will assume $\mathrm{Re}_{Tpx}$ and $\mathrm{Re}_{Tpy}$ to be given (say, as a percentage of $\mathrm{Re}_0$) and investigate the consequences of such particle-velocity fluctuation on the average drag force.

## C. Enhanced undisturbed fluid-velocity fluctuation

First, we investigate the influence of particle-velocity fluctuation on particle-to-particle variation in the undisturbed fluid velocity. Consider the $i$th particle surrounded by its neighbors in the stationary case versus the nonstationary case. Let the instantaneous location of the neighbors be the same and let the macroscale fluid velocity be the same in both cases. In the stationary case,

the perturbation flow induced by the $j$th neighbor depends only on the undisturbed fluid flow at its location, whereas in the nonstationary case the perturbation flow induced by the $j$th neighbor will additionally depend on the velocity of the $j$th particle.[4] Changes in the magnitude and orientation of the perturbation flow of all the neighbors, due to their motion, will impact the undisturbed flow of the $i$th particle.

As a simple example consider an upstream neighbor of the $i$th particle, under both the stationary condition and when the upstream neighbor is moving farther upstream (downstream) relative to the $i$th particle, on a sufficiently rapid timescale. Due to its upstream (downstream) motion, the relative velocity and the perturbation flow of the neighbor will be stronger (weaker) in the nonstationary scenario. In turn, the wake effect of the upstream neighbor on the $i$th particle will be stronger (weaker). However, when we superpose the perturbation flow of all the neighbors and consider the resulting undisturbed fluid flow of a distribution of particles, it is not readily apparent by how much the resulting distribution of undisturbed fluid flow will differ from that of the stationary particles presented in Fig. 2.

We therefore revisit the scenario of a random distribution of particles in a large triply periodic box considered in Sec. III. As before, the random spatial locations of the particles within the box are chosen with uniform probability. The different volume fractions and Reynolds numbers considered are the same as those presented in Table I. Though the distribution of particles in each realization remains the same as in the stationary counterpart, the particles are now in motion and therefore the chosen particle locations represent their position at one time instant. A uniform mean pressure gradient is applied along the mean flow direction ($x$ axis). Again the length scale of the box filter is the same as the periodic box and as a result the macroscale quantities are homogeneous.

Each particle within the periodic box is given a random velocity, obeying the following properties. (i) The mean particle velocity is zero. In other words, the frame of reference is attached to the mean particle motion. (ii) Each component of each particle's velocity is a random variable of Gaussian distribution. The rms values of the normalized particle-velocity variation are given by $\mathrm{Re}_{Tpx}$, $\mathrm{Re}_{Tpy}$, and $\mathrm{Re}_{Tpz}$. (iii) Each particle's velocity is uncorrelated from that of all others. (iv) For now we will assume particle-velocity variation to be isotropic (i.e., $\mathrm{Re}_{Tpx} = \mathrm{Re}_{Tpy} = \mathrm{Re}_{Tpz} = \mathrm{Re}_{TP}$). Such a Maxwellian particle-velocity distribution has been considered by others [39,41]. The problem is then characterized by three parameters: the macroscale Reynolds number $\mathrm{Re}_0$, the constant particle volume fraction $\phi_0$, and $\mathrm{Re}_{TP}$. Particle-resolved simulations of this scenario have been considered in [39,40], where a steady flow solution was obtained around a random distribution of particles. Though the particles did not move in the simulation, a nonzero random velocity was applied as a boundary condition at each particle.

The microscale undisturbed velocity of each particle now depends on the precise arrangement of its neighbors and their velocities. Again, the distributions of $\boldsymbol{u}_{\mathrm{mic@i}}$ both along the flow direction and along the transverse direction are of interest. Following (17), the microscale contribution to undisturbed flow velocity is approximated by a superposition of surface averages of superposable wakes of nearby neighbors. Normalized histograms of $u_{\mathrm{mic@i,x}}/U_0$ and $u_{\mathrm{mic@i,y}}/U_0$ are shown in Fig. 7 for the same three different combinations of $\mathrm{Re}_0$ and $\phi_0$ considered earlier in Fig. 2 for the stationary particles. The figure shows the results for the particular case when $\mathrm{Re}_{TP}/\mathrm{Re}_0 = 0.5$. Also plotted as red lines in all the figures are the best-fitting PDFs of the histograms.

It can be observed that compared to the stationary case the level of particle-to-particle variation in the undisturbed flow velocity has increased substantially. The increase is observed in both the streamwise and the transverse components. The width of the distribution increases with $\mathrm{Re}_0$ and $\phi_0$. While the distributions are closely Gaussian in shape at the higher volume fraction, the streamwise distribution follows a shifted $\Gamma$ distribution at lower volume fraction with positive skewness. The

---

[4]Technically, if the velocity of the $i$th and the $j$th particle are the same, the $j$th particle is considered stationary with respect to the $i$th particle.
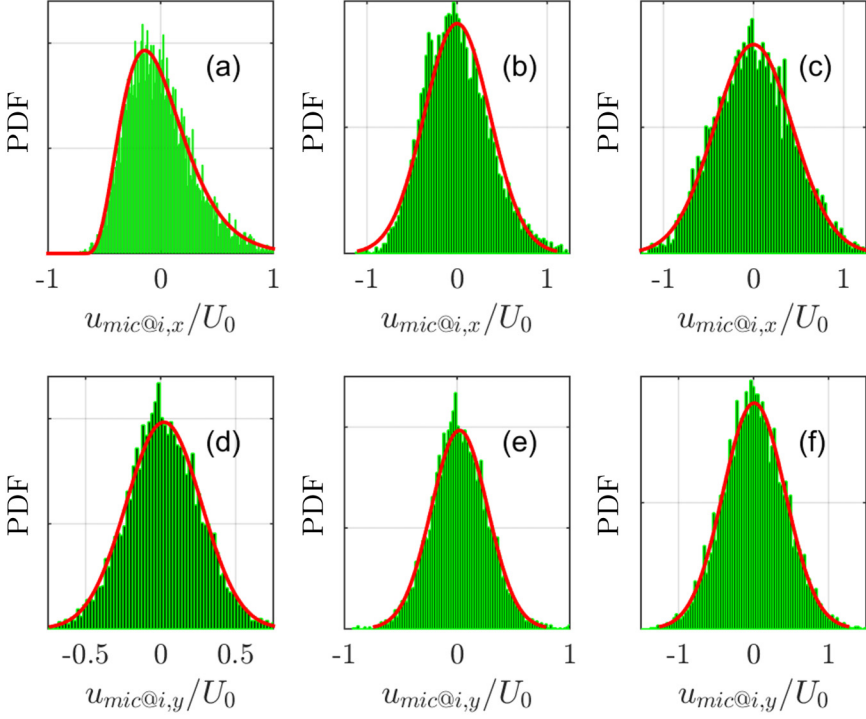
FIG. 7. Results for the nonstationary case with the normalized particle-velocity fluctuation $\mathrm{Re}_{Tp}/\mathrm{Re}_0 = 0.5$: normalized histograms of (a)–(c) the streamwise component of the surface averaged undisturbed velocity fluctuation at the particles and (d)–(f) the transverse component of the undisturbed velocity fluctuation at the particles for (a) and (d) $\mathrm{Re}_0 = 100$ and $\phi_0 = 0.11$, (b) and (e) $\mathrm{Re}_0 = 60$ and $\phi_0 = 0.21$, and (c) and (f) $\mathrm{Re}_0 = 30$ and $\phi_0 = 0.45$. In all the plots the red curve shows the best-fitting analytical distribution. In (a) the best fit is a $\Gamma$ distribution, while in the others a Gaussian fit is shown.

enhanced asymmetric nature of the distribution at low volume fraction is due to the increased fore-aft asymmetry of the wake at finite Reynolds numbers. Plots similar to Fig. 3 were considered to establish that there is no systematic correlation between the streamwise and transverse components.

The microscale undisturbed velocity of all $N$ particles within the system is then used to calculate the rms Reynolds-number fluctuation as given in (26). Figure 8 shows plots of $\mathrm{Re}_{Tfx}/\mathrm{Re}_{Tfx0}$ and $\mathrm{Re}_{Tfy}/\mathrm{Re}_{Tfy0}$ for a range of macroscale Reynolds numbers. The three frames show the results for three different volume fractions considered. Here $\mathrm{Re}_{Tfx0}$ and $\mathrm{Re}_{Tfy0}$ correspond to the rms normalized undisturbed fluid-velocity fluctuation in the stationary particle limit. Thus, in Fig. 8 the ordinate corresponds to an increase in the undisturbed fluid-velocity fluctuation due to particle motion. In each frame the three different colors correspond to $\mathrm{Re}_{Tp}/\mathrm{Re}_0 = 0.1, 0.3$, and $0.5$. From the figure it appears that the increase is independent of the macroscale Reynolds number and the increase of the transverse component is larger than the streamwise component. In the dilute limit of $\phi_0 \to 0$ we expect the microscale contribution to the undisturbed fluid velocity of a particle to approach zero, due to the lack of neighbor influence. Thus, in this limit $\mathrm{Re}_{Tfx}, \mathrm{Re}_{Tfy} \to 0$, independently of the magnitude of particle-velocity fluctuation. At finite volume fraction, the effect of particle-velocity fluctuation appears to initially increase with volume fraction and saturate above $\phi_0 \approx 0.2$ in the case of the streamwise component. In the case of the transverse component the variation with volume fraction is not significant. It can also be noted that the increase in $\mathrm{Re}_{Tfy}$ is substantially larger than in $\mathrm{Re}_{Tfx}$. Thus, compared to Figs. 4(a) and 4(b) for the stationary case, where the ratio of the streamwise component to the transverse component was much larger than
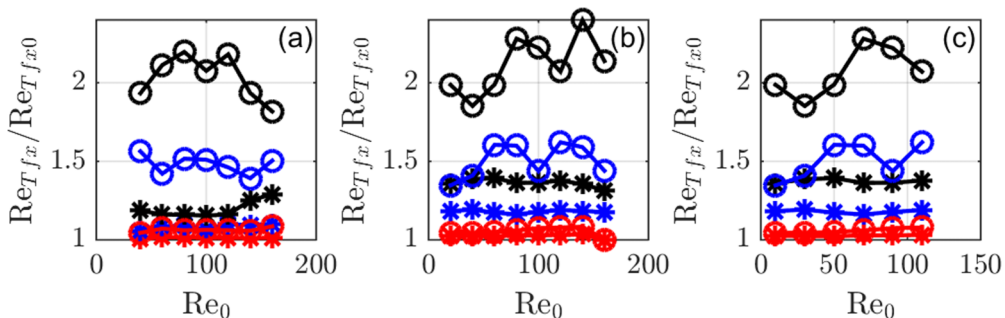
FIG. 8. Plot of increase in rms normalized streamwise and transverse undisturbed fluid-velocity fluctuation due to particle motion for (a) $\phi_0 = 0.11$, (b) $\phi_0 = 0.21$, and (c) $\phi_0 = 0.45$. The ratios $\text{Re}_{Tfx}/\text{Re}Tfx0$ (stars) and $\text{Re}_{Tfy}/\text{Re}_{Tfy0}$ (circles) are plotted, where $\text{Re}_{Tfx0}$ and $\text{Re}_{Tfy0}$ correspond to rms normalized microscale undisturbed fluid-velocity fluctuation in the stationary particle limit. In each frame red, blue, and black correspond to $\text{Re}_{Tp}/\text{Re}_0 = 0.1$, 0.3, and 0.5, respectively.

unity, in the case of nonstationary particles the streamwise and transverse undisturbed fluid-velocity components begin to approach each other with increasing particle-velocity variation. This can be anticipated, since the preferred orientation of the particle wakes along the $x$ direction in the case of stationary particles is substantially modified with the introduction of random particle motion and isotropy is recovered.

### D. Eulerian force model (nonstationary)

We now consider the Eulerian modeling of force averaged over the local filter volume for the case of moving particles. The definition of the Eulerian normalized average force given in (28) still applies (without the subscript 0, since particles are not stationary). We now proceed to apply the best available model for the force of the $i$th particle. We assume $\boldsymbol{F}_i$ to be well modeled by

$$\boldsymbol{F}_i = 3\pi \mu d (\boldsymbol{u}_{@i} - \boldsymbol{v}_i) \Phi_0^L (\text{Re}_{@i}, \phi_0). \tag{39}$$

Here both the Stokes drag and the function $\Phi_0^L$ are based on the relative velocity between the undisturbed fluid flow and the particle velocity. The above expression is an approximation, since it uses the Lagrangian correlation $\Phi_0^L$ even in the present scenario of nonstationary particles. We recall that $\Phi_0^L$ was earlier defined in the limit of stationary particles. In fact, the observation in [42] that their DNS force on the particles is larger than that predicted with the EE force model of [2] suggests that $\Phi^L$ under the nonstationary condition is likely to be higher than $\Phi_0^L$, at least for the specific case that they considered. Nevertheless, it must be stressed that in the present approach particle-to-particle variation in both the particle velocity and the undisturbed fluid velocity is taken into account through the proper definition of relative velocity.

We now revisit the cases considered in Figs. 7 and 8. Since the particle velocity is imposed (as opposed to being decided by free motion), the correlation between particle velocity and the undisturbed fluid velocity is zero. This lack of correlation is appropriate only in the case of large inertia particles, which do not respond to fluid-velocity fluctuations, or when the particle dynamics is dominated by interparticle collisions. At low values of particle inertia, the particle velocity will be correlated with its undisturbed fluid velocity. We now use the model presented in (33) for $\Phi_0^L$ in (39) and evaluate the Eulerian normalized average force given in (28). Figure 9 shows plots of $\Phi^E$ thus calculated for a range of $\text{Re}_0$, for $\text{Re}_{Tp}/\text{Re}_0 = 0.0, 0.1, 0.3$, and 0.5. The results for four different values of $\phi_0 = 0.0, 0.11, 0.21$, and 0.45 are shown in different frames.

Also shown in the figures as black dashed lines are the corresponding plots of $\Phi_0^L$ as a function $\text{Re}_0$, which corresponds to the Lagrangian drag on an individual particle whose Reynolds number
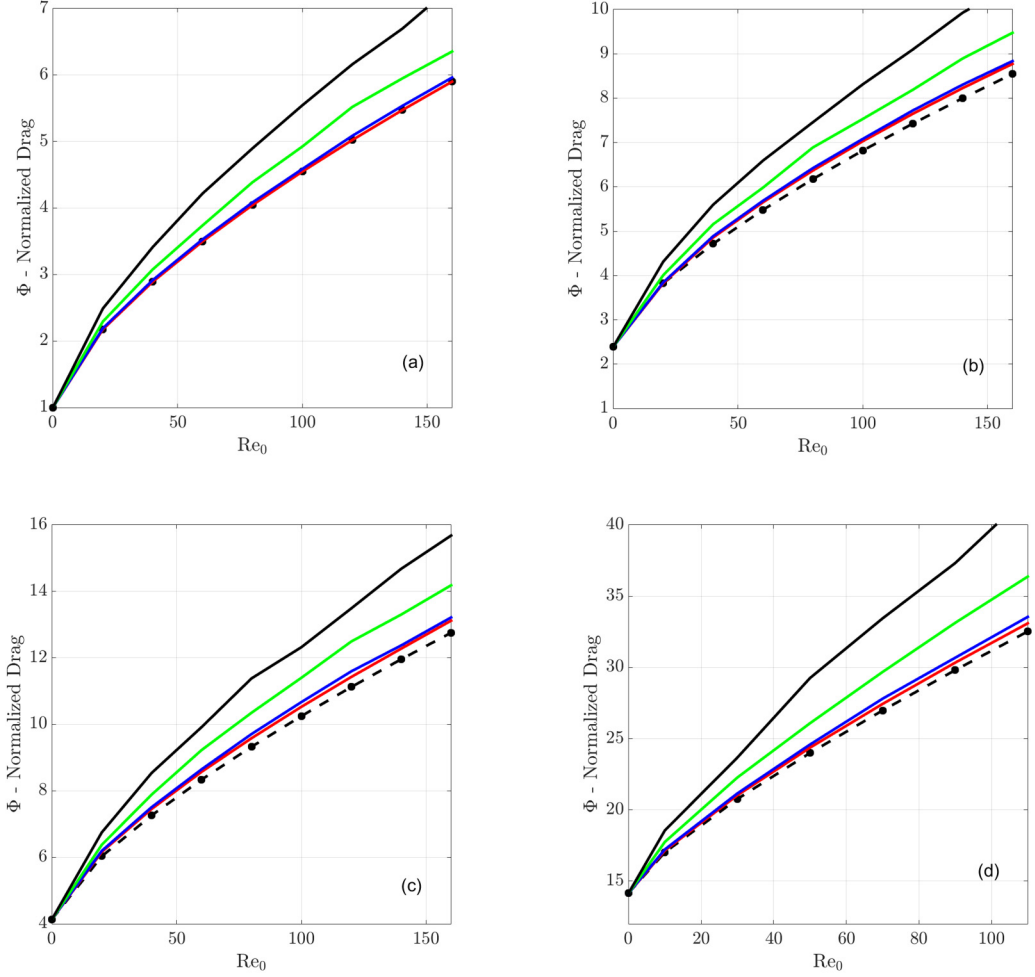
FIG. 9. Eulerian normalized average force $\Phi^E$ plotted as a function of macroscale Reynolds number $\mathrm{Re}_0$ for (a) $\phi_0 = 0.0$, (b) $\phi_0 = 0.11$, (c) $\phi_0 = 0.21$, and (d) $\phi_0 = 0.45$. The black dashed line corresponds to $\Phi_0^L$. The different solid lines in each frame correspond to different values of particle-velocity fluctuation: red, $\mathrm{Re}_{Tpx}/\mathrm{Re}_0 = 0.0$; blue, $\mathrm{Re}_{Tpx}/\mathrm{Re}_0 = 0.1$; green, $\mathrm{Re}_{Tpx}/\mathrm{Re}_0 = 0.3$; and black, $\mathrm{Re}_{Tpx}/\mathrm{Re}_0 = 0.5$. In all these cases the particle-velocity fluctuation is isotropic (i.e., $\mathrm{Re}_{Tpx} = \mathrm{Re}_{Tpy}$).

and local volume fraction are $\mathrm{Re}_0$ and $\phi_0$, respectively. The red line corresponds to the stationary limit of zero particle velocity and thus is identical to the plot of $\Phi_0^E$. As was discussed in the context of Fig. 5, the difference is due to averaging over the stationary particles whose Reynolds number varies due to variation in the undisturbed fluid velocity. In the limit of zero volume fraction $\Phi_0^L$ and $\Phi_0^E$ are identical.

With increasing particle-velocity variation we see that there is a substantial increase in the Eulerian average. This increase vanishes in the Stokes limit of $\mathrm{Re}_0 \rightarrow 0$ and is amplified at finite Reynolds number. In the zero-volume-fraction limit, since each particle is unaffected by all other particles, the difference between $\Phi^E$ and $\Phi_0^L$ is entirely due to particle-velocity variation, whereas at finite $\phi_0$ the increase in Eulerian average is due to both particle-velocity variation and undisturbed fluid-velocity variation. Such an increase in drag due to added particle motion has previously been reported based on the results of finite-Re PR simulations [39–41]. It must however be cautioned
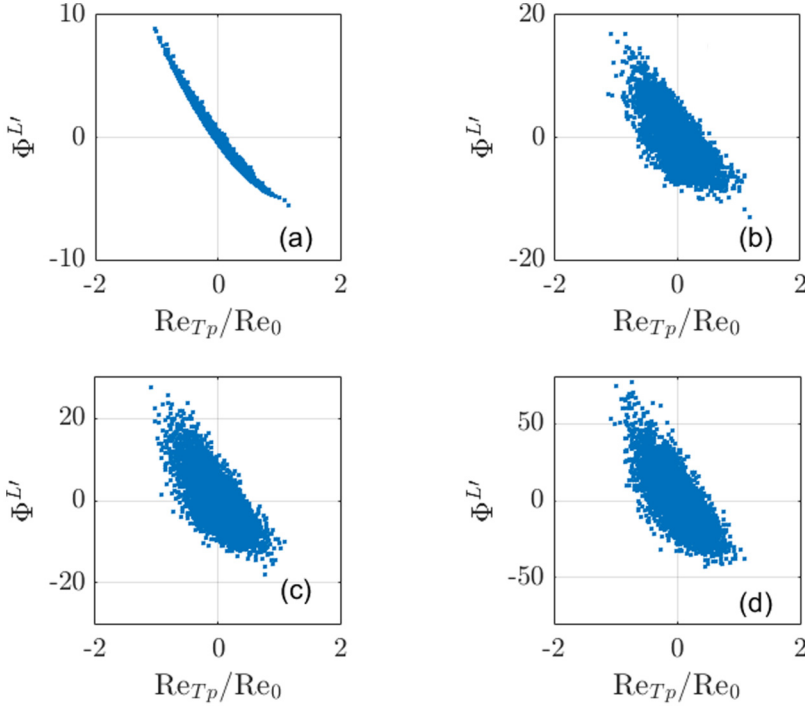
FIG. 10. Scatter plot of normalized streamwise force deviation of a particle away from the average as a function of the streamwise component of the particle velocity for (a) $\phi_0 = 0.0$, (b) $\phi_0 = 0.11$, (c) $\phi_0 = 0.21$, and (d) $\phi_0 = 0.45$.

that this increase is when the particle-velocity variation is uncorrelated with the undisturbed fluid-velocity variation. Under conditions of freely moving particles of low Stokes number, the correlation between the fluid and particle-velocity variation greatly reduces the relative velocity variation. In fact, as a result of correlation, the average drag can fall below that of the stationary limit as illustrated in the cases considered in [31].

The Eulerian average force under the stationary condition $\Phi_0^E$ (represented by the red solid line in Fig. 9) is the appropriate quantity that should be compared with the average drag as obtained in the PR DNSs of [2,3,6,7,9,10]. In contrast, classic drag laws such as those given in [4,5,8] are based on freely moving particles and therefore should be compared to one of the $\Phi^E$ curves given in Fig. 9 with the appropriate value of particle-velocity fluctuation. It should be cautioned that for a proper comparison, however, one must also include a nonuniform distribution of particles and anisotropy in the nature of the particle-velocity variation. Nevertheless, it is clear that the Eulerian average of a freely moving assembly of particles will be higher than that obtained under the stationary condition.

Figure 10 presents scatter plots of the variation in the normalized streamwise force of a particle away from its average as a function of the streamwise component of particle velocity. Here $\Phi^{L\prime} = \Phi^L - \langle \Phi^L \rangle$, where the angular brackets represent an average aver all the particles. The results are plotted for the four volume fractions considered at $\mathrm{Re}_0 \approx 100$ and in all cases $\mathrm{Re}_{Tp}/\mathrm{Re}_0 = 0.3$. These results are in good agreement with those shown in [40] based on their PR simulations. As can be expected, there is a negative correlation between the streamwise particle velocity and the streamwise drag, since as the particle velocity increases the relative velocity decreases. In the zero-volume-fraction limit, there is a very good correlation between the streamwise velocity variation and the streamwise force, and the lack of a perfect correlation is due to particle-velocity variation along the transverse directions; however, the correlation between $\Phi^{L\prime}$ and $\mathrm{Re}_{Tp}/\mathrm{Re}_0$ weakens at finite

volume fraction. This is due to the fact that the undisturbed velocity of each particle is influenced by the particle velocity of its neighbors. In fact, as pointed out in [40], there are instances when the streamwise component of the particle velocity is positive (negative) and the corresponding effect on the streamwise force is positive (negative). Clearly, for such particles the increase (decrease) in streamwise drag must be due to an increase (a decrease) in the undisturbed fluid velocity.

### 1. Simple model of $\Phi^E$

We now present a simple model for the nonstationary Eulerian average force $\Phi^E$ as a function of the macroscale parameters $\mathrm{Re}_0$, $\phi_0$, $\mathrm{Re}_{Tpx}$, and $\mathrm{Re}_{Tpy}$. We obtain this relation by substituting Eq. (39) into (28) and following the steps pursued in (36) to get

$$\Phi^E = \Phi_0^L(\mathrm{Re}_0, \phi_0) + \left[\frac{1}{2}\frac{\partial^2 \hat{\Phi}_0^L}{\partial \mathrm{Re}_{@ix}^2}\right]_0 \mathrm{Re}_{Tx}^2 + \left[\frac{\partial^2 \hat{\Phi}_0^L}{\partial \mathrm{Re}_{@iy}^2}\right]_0 \mathrm{Re}_{Ty}^2. \qquad (40)$$

In obtaining the above we have defined the mean square fluctuation in the streamwise Reynolds number to be $\mathrm{Re}_{Tx}^2 = \frac{1}{N}\sum_{i=1}^{N}(\mathrm{Re}_{@ix} - \mathrm{Re}_0)^2$, with a similar definition for the transverse component. We now use (37) to replace the terms within the square brackets to obtain

$$\Phi^E = \Phi_0^L(\mathrm{Re}_0, \phi_0) + (\Phi_0^E - \Phi_0^L)g_x\left(\frac{\mathrm{Re}_{Tx}}{\mathrm{Re}_{Tfx0}}\right)^2 + (\Phi_0^E - \Phi_0^L)(1 - g_x)\left(\frac{\mathrm{Re}_{Ty}}{\mathrm{Re}_{Tfy0}}\right)^2, \qquad (41)$$

where the fractional contribution to force enhancement from the streamwise undisturbed fluid-velocity variation of the stationary configuration (i.e., $g_x$) was defined in (37). The second and third terms on the right-hand side account for the increase in Eulerian average over the Lagrangian estimation due to averaging of the nonlinear drag relation. Part of it comes from variation in the streamwise relative velocity, represented by the second term, and part comes from variation in the transverse component of relative velocity, represented by the third term. In the limit of stationary particles, $\mathrm{Re}_{Tx} \to \mathrm{Re}_{Tfx0}$ and $\mathrm{Re}_{Ty} \to \mathrm{Re}_{Tfy0}$ and as a result, according to the above relation, $\Phi^E$ will correctly approach $\Phi_0^E$. In the case of freely moving particles, the difference $\Phi^E - \Phi_0^E$ will depend not only on $\mathrm{Re}_0$ and $\phi_0$, but also on how much streamwise and transverse relative velocity variations within the averaging volume have amplified their values for the stationary limit.

Relative velocity variation is due to both the undisturbed velocity variation and the particle-velocity variation. It can be readily shown that

$$\left(\frac{\mathrm{Re}_{Tx}}{\mathrm{Re}_{Tfx0}}\right)^2 = \left(\frac{\mathrm{Re}_{Tfx}}{\mathrm{Re}_{Tfx0}}\right)^2 + \left(\frac{\mathrm{Re}_{Tpx}}{\mathrm{Re}_{Tfx0}}\right)^2 - 2\left(\frac{\mathrm{Re}_{Tfpx}}{\mathrm{Re}_{Tfx0}}\right)^2,$$

$$\left(\frac{\mathrm{Re}_{Ty}}{\mathrm{Re}_{Tfy0}}\right)^2 = \left(\frac{\mathrm{Re}_{Tfy}}{\mathrm{Re}_{Tfy0}}\right)^2 + \left(\frac{\mathrm{Re}_{Tpy}}{\mathrm{Re}_{Tfy0}}\right)^2 - 2\left(\frac{\mathrm{Re}_{Tfpy}}{\mathrm{Re}_{Tfy0}}\right)^2, \qquad (42)$$

where the fluctuation Reynolds numbers of the undisturbed fluid-velocity variation ($\mathrm{Re}_{Tfx}$ and $\mathrm{Re}_{Tfy}$), particle-velocity variation ($\mathrm{Re}_{Tpx}$ and $\mathrm{Re}_{Tpy}$), and their correlations have been defined in (21)–(24).

The general expression (41) for the Eulerian force correlation $\Phi^E$ has been mechanistically developed with the intension of broad applicability in a wide variety of multiphase flows. However, its utility clearly depends on our ability to model the three ratios that appear on the right-hand side of (42). The ratios $\mathrm{Re}_{Tfx}/\mathrm{Re}_{Tfx0}$ and $\mathrm{Re}_{Tfx}/\mathrm{Re}_{Tfx0}$ measure amplification of the rms streamwise and transverse undisturbed fluid-velocity variation due to particle motion. Based on the results presented in Fig. 8, these ratios are larger than unity and the increase is more substantial for the transverse component. These ratios, when taken to be approximately independent of $\mathrm{Re}_0$, are shown in Fig. 11 as a function of $\mathrm{Re}_{Tpx}/\mathrm{Re}_0$. The results are presented for the three different volume fractions considered. The second term of the streamwise component can be better quantified by
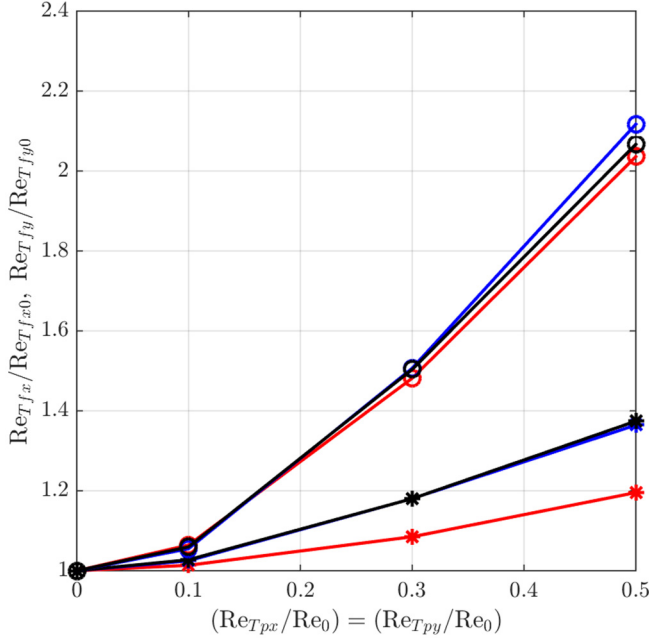
FIG. 11. Plot of the ratios $\mathrm{Re}_{Tfx}/\mathrm{Re}_{Tfx0}$ and $\mathrm{Re}_{Tfy}/\mathrm{Re}_{Tfy0}$ as a function of $\mathrm{Re}_{Tpx}/\mathrm{Re}_0 = \mathrm{Re}_{Tpx}/\mathrm{Re}_0$ for the three different volume fractions $\phi_0 = 0.11$ (red), $\phi_0 = 0.21$ (blue), and $\phi_0 = 0.45$ (black). Stars correspond to the streamwise component and circles to the transverse component.

rewriting it as

$$\frac{\mathrm{Re}_{Tpx}}{\mathrm{Re}_{Tfx0}} = \frac{\mathrm{Re}_{Tpx}/\mathrm{Re}_0}{\mathrm{Re}_{Tfx0}/\mathrm{Re}_0}. \tag{43}$$

In the example considered in Fig. 9 the numerator is an input whose value was varied from 0% to 50%. The denominator pertains to the stationary particle case and its variation with $\mathrm{Re}_0$ and $\phi_0$ was presented in Fig. 4.

The correlation between the particle and undisturbed fluid-velocity variation represented by the last term is quite important, since a positive correlation can reduce the additive effect of the particle and undisturbed fluid-velocity variation. The results presented in Fig. 9 are based on the assumption of zero correlation employed in that example problem. This assumption is applicable for regime-III particles of large Stokes number which do not respond to any of the turbulent eddies. As a result, the particle-velocity variation is uncorrelated from its undisturbed fluid-velocity variation. However, in other applications involving freely moving particles of smaller Stokes number, the correlation will be nonzero and its contribution can be so large that the Reynolds number of the relative velocity fluctuation can decrease below that of the stationary limit. This point is tested in Fig. 12, where we reconsider the problem studied in Fig. 9. Earlier, each particle of the random distribution was given a random velocity of the Maxwellian distribution that was completely uncorrelated from the undisturbed fluid velocity of the particle. In the present test, each particle of the distribution is given a random velocity of Maxwellian distribution, whose correlation with the undisturbed fluid velocity was systematically changed (i.e., $C = 0.0, 0.25, 0.5, 0.75,$ and $1.0$). The Eulerian normalized average forces $\Phi^E$ for these cases are shown as solid and dashed lines in Fig. 12. Also plotted in the figure are $\Phi^L(\mathrm{Re}_0)$ as the black crosses and $\Phi^E(\mathrm{Re}_0)$ as the blue crosses. It is clear from the figure that with increasing correlation, the Eulerian average drag decreases, since particle-to-particle variation of relative velocity decreases. As can be expected, under perfect
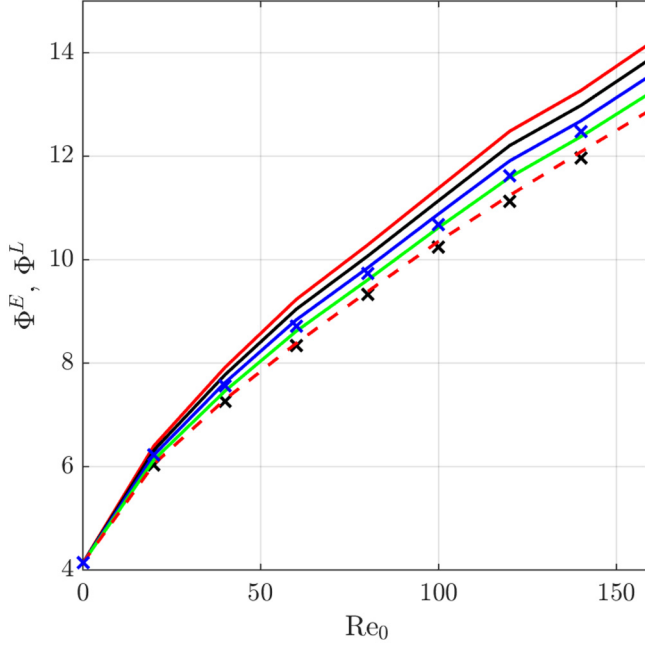
FIG. 12. Plot of $\Phi^E$ investigating the effect of correlation between the particle-velocity variation with the undisturbed fluid-velocity variation for correlation values of $C = 0.0$ (red solid line), 0.25 (black solid line), $C = 0.5$ (blue solid line), $C = 0.75$ (green solid line), and $C = 1.0$ (red dashed line). Also plotted are $\Phi^L(\text{Re}_0)$ (black crosses) and $\Phi^E(\text{Re}_0)$ (blue crosses). The results are for $\phi_0 - 0.21$.

correlation (i.e., $C = 1.0$) the deviation of the undisturbed fluid velocity of each particle from the average is perfectly compensated by the deviation of its particle velocity and results in very little deviation in its Reynolds number from the average value of $\text{Re}_0$. This is the reason why the red dashed line of $C = 1.0$ is in excellent agreement with the black crosses of $\Phi^L(\text{Re}_0)$. Thus, under perfect correlation, the Eulerian normalized average force of freely moving particles can be lower than that for a stationary system. Such behavior was observed in the simulations of [31]. It is interesting to note that at a correlation of around 0.75, $\Phi^E$ for the nonstationary system becomes approximately the same as $\Phi_0^E$.

The increase in normalized Eulerian average force due to particle motion can be explicitly expressed using (41) as

$$\Phi^E - \Phi_0^E = (\Phi_0^E - \Phi_0^L)g_x\left(\frac{\text{Re}_{Tx}^2}{\text{Re}_{Tfx0}^2} - 1\right) + (\Phi_0^E - \Phi_0^L)(1 - g_x)\left(\frac{\text{Re}_{Ty}^2}{\text{Re}_{Tfy0}^2} - 1\right), \qquad (44)$$

which can be compared with prior predictions based on PR simulations in [39,43]. Tang *et al.* [43] considered freely moving suspensions of particles of varying particle-to-fluid density ratio and predicted the increase in normalized drag to be proportional to $\text{Re}_{Tp}$. However, the value of $\text{Re}_{Tp}/\text{Re}_0$ realized in their simulations was quite small. The PR simulations of [39] closely match the example problem considered here. Huang *et al.* proposed a model where the increase in Eulerian normalized average force is expressed as proportional to $\text{Re}_{Tp}^{1.49}$. The quadratic dependence of the model presented in Eq. (41) is a consequence of the Taylor series expansion, and this scaling corresponds well with the low-Reynolds-number model advanced in [41]. However, $\Phi^E$ in (41) depends on a change in the Reynolds number based on the relative velocity variation, for which $\text{Re}_{Tp}$ is only one of three contributors [see (42)]. The Eulerian normalized average force may increase
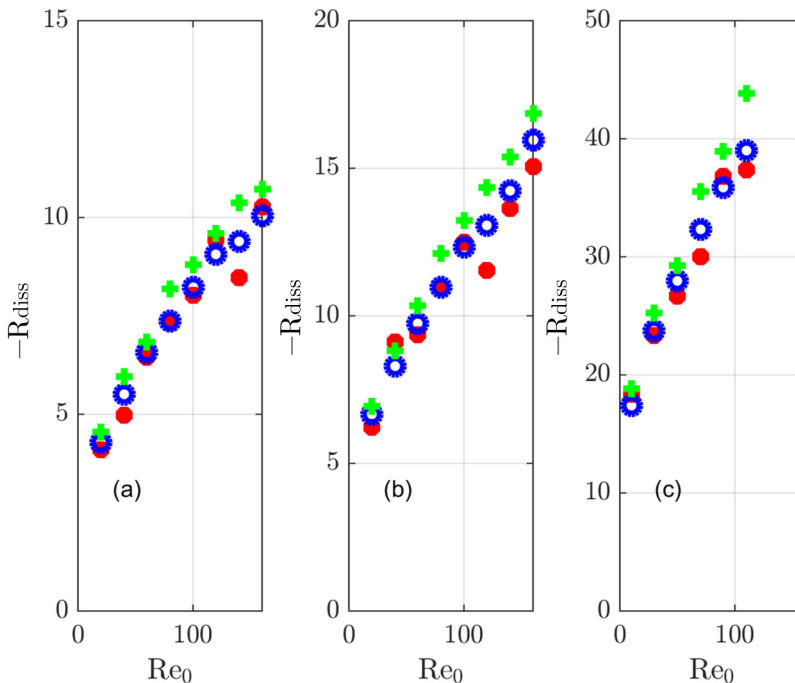
FIG. 13. Plot of $-R_{\mathrm{diss}}$ versus $\mathrm{Re}_0$ for $\mathrm{Re}_{Tp}/\mathrm{Re}_0 = 0.1$, 0.3, and 0.5 and volume fraction values (a) $\phi_0 = 0.11$, (b) $\phi_0 = 0.21$, and (c) $\phi_0 = 0.45$.

or decrease depending on the relation between the particle-velocity variation and the undisturbed fluid-velocity variation. The results of [39,43] are useful for the configurations they studied.

The relation between the $\Phi^E$ model given in (41) and the granular temperature equation must be recognized. Particle-velocity fluctuation as predicted by the granular temperature equation is the key input. Particle-velocity fluctuation in turn influences the distribution of undisturbed fluid-velocity fluctuation, and their correlation also depends on the response time of the particles. The resulting mean hydrodynamic force on the particles as predicted by $\Phi^E$ is then the source of fluid-mediated dissipation in the granular temperature equation. Following [41], we define the nondimensional dissipation of the granular temperature as

$$R_{\mathrm{diss}} = \frac{1}{9\pi \mu d v_{\mathrm{rms}}^2} \frac{1}{N} \sum_{i=1}^{N} \boldsymbol{F}_i \cdot \boldsymbol{v}_i, \tag{45}$$

where the velocity of the $i$th particle is $\boldsymbol{v}_i$, whose mean is chosen to be zero and the rms particle-velocity fluctuation is taken to be the same along all three directions (i.e., $v_{\mathrm{rms},x} = v_{\mathrm{rms},y} = v_{\mathrm{rms},z} = v_{\mathrm{rms}}$). Plots of $R_{\mathrm{diss}}$ as a function of $\mathrm{Re}_0$ are shown in Fig. 13 for the three different volume fractions and for the three different values of $\mathrm{Re}_{Tp}/\mathrm{Re}_0 = 0.1$, 0.3, and 0.5. These results can be compared with the corresponding results of the $\phi_0 = 0$ limit. In this very dilute limit, the undisturbed flow of each particle is simply the macroscale uniform flow and thus fluctuation in force is entirely due to particle-velocity variation. Furthermore, in the dilute limit, the standard drag correlation applies. With these facts and using a Taylor series expansion, the leading-order expression of $R_{\mathrm{diss}}$ can be obtained as

$$R_{\mathrm{diss}} \approx -2 - 0.3687 \, \mathrm{Re}_0^{0.687} \quad \text{for } \phi_0 = 0, \tag{46}$$

which can be compared with the results presented in Fig. 13. In the dilute limit $R_{\text{diss}}$ is independent of the ratio $\text{Re}_{Tp}/\text{Re}_0$ and this lack of dependence appears to hold at finite volume fractions at lower values of $\text{Re}_{Tp}/\text{Re}_0$. A small increase in $R_{\text{diss}}$ can be noticed at the high fluctuation level of $\text{Re}_{Tp}/\text{Re}_0 = 0.5$. The increase in $R_{\text{diss}}$ with increasing volume fraction is due to both an increase in mean drag and an increase in the distribution of relative velocity due to undisturbed fluid-velocity fluctuations. Figure 13 applies only in the case of uncorrelated undisturbed fluid and particle-velocity fluctuations. We expect the magnitude of $R_{\text{diss}}$ to decrease in the case of low-inertia particles whose undisturbed fluid and particle-velocity fluctuations will be correlated.

### E. Lagrangian force model (nonstationary)

We finally consider the Lagrangian force model for use in EL simulations of freely moving particles. Here again we distinguish between the two different EL approaches: EL-mac and EL-mic. As seen in Fig. 8, as a result of particle motion, even the variation in undisturbed fluid velocity increases. Particle-to-particle variation in both the particle velocity and the undisturbed fluid velocity contributes to enhanced variation in the particle Reynolds number based on the relative velocity and in turn to larger variation in particle force. In the EL-mic approach, each particle is informed not only of its velocity but also of the undisturbed fluid velocity of the particle, including the microscale contribution of its neighbors. In other words, both $\boldsymbol{v}_i$ and $\boldsymbol{u}_{@i}$ are known for each particle being tracked in the EL-mic approach. The force of the particle can then be easily evaluated using (33).

In the case of the EL-mac approach, only the macroscale component of the undisturbed flow is available. As a consequence, particle-to-particle variation in undisturbed flow is greatly underestimated. Furthermore, we can expect the particle-velocity variation to be lower than in a PR DNS or EL-mic simulation. Therefore, similar to (39), we define the Lagrangian force on a particle as

$$\boldsymbol{F}_i = 3\pi \mu d(\boldsymbol{u}_{\text{mac}@i} - \boldsymbol{v}_i)\Phi_{LE}(\text{Re}_{\text{mac}@i}, \phi_0). \tag{47}$$

The function $\Phi^{LE}$ in the above expression is different from $\Phi_0^L$ that appears in (39), since it must account for the effect of enhanced variation in relative velocity. In particular, just like $\Phi^E$, $\Phi^{LE}$ must also be a function of $\text{Re}_{Tpx}$. The consistency requirement can be enforced by substituting the above into the right-hand side of (28) and requiring that it be equal to the nonstationary Eulerian average drag $\Phi^E$ obtained in the preceding section and presented in Fig. 9. In other words, we demand that the macro-Lagrangian force $\Phi^{LE}$, when applied to individual particles in an EL-mac simulation and averaged over the distribution of particles within the averaging volume, should equal the Eulerian average. This is an inverse problem which can be solved to obtain the correct macro-Lagrangian force. Provided the averaging filter length is much larger than the particle size, we can expect $\Phi^{LE}$ to approach the Eulerian average force model $\Phi^E$.

## V. DISCUSSION AND CONCLUSIONS

One of the insights presented in this work is information on the undisturbed fluid velocity of a random distribution of particles subjected to a uniform macroscale flow. The undisturbed flow of a particle is of fundamental importance since it controls both the undisturbed flow force (also known as pressure gradient or Archimedes force) and the quasisteady force. An easy way to calculate the undisturbed flow of a particle is lacking since it requires a particle-resolved simulation in the absence of that particle but in the presence of all other particles. Here we used the pairwise interaction extended point particle framework of [11,12,33] to evaluate the undisturbed flow of each particle through superposition of the perturbation flow induced by all its neighbors. This approach has allowed us the opportunity to obtain various statistics related to undisturbed fluid velocity under conditions of both stationary and nonstationary particles.

TABLE II. List of all the normalized force expressions presented in this work. Here it is assumed that in the EL-macro approach the filter length scale is sufficiently larger than the particle size, so it is essentially similar to the EE approach.

| Simulation methodology | Force law (stationary) | Force law (nonstationary) |
| --- | --- | --- |
| Euler-Euler | $\Phi_0^E$ = Eq. (29) | $\Phi^E$ = Eq. (41) |
| Euler-Lagrange–micro | $\Phi_0^L$ = Eq. (33) | $\Phi^L \approx$ Eq. (33) |
| Euler-Lagrange–macro | $\Phi_0^{LE} \approx$ Eq. (29) | $\Phi^{LE} \approx$ Eq. (41) |

In a random distribution of particles, even though the macroscale flow of all the particles is the same, it was observed that the microscale undisturbed flow that arises due to the perturbation flow of neighbors varies substantially from particle to particle, and this in turn leads to large variation in the hydrodynamic force exerted on the particles. Even in the case of stationary particles, there is substantial particle-to-particle variation in both the streamwise and transverse components of the undisturbed fluid velocity. The variation in the streamwise velocity component is much larger than the variation in the transverse component. The variation as a percentage of the macroscale velocity decreases with increasing macroscale Reynolds number. When particles are allowed to move and given random velocity, the effect of particle motion is to increase the particle-to-particle variation in the undisturbed fluid velocity of the particles. This increase is greater for the transverse component than for the streamwise component. As a result, with increasing random particle motion, the influence of the preferred direction of the macroscale flow decreases and as a result the distribution of undisturbed fluid-velocity fluctuation approaches isotropy.

Three different normalized forces have been defined for the evaluation of the hydrodynamic force on the particle: $\Phi^L$ is the Lagrangian normalized force on an individual particle that is suitable for application in an Euler-Lagrange simulation, where particle-to-particle variation in the undisturbed fluid velocity has been accounted for either in a deterministic or in a stochastic manner; $\Phi^E$ is the Eulerian normalized average force on all the particles within the averaging volume suitable for application in an Euler-Euler simulation; and $\Phi^{LE}$ is the Lagrangian normalized force on an individual particle that is suitable for application in an Euler-Lagrange simulation, where only the macroscale undisturbed fluid velocity is used in calculating the particle force.

An important result of the present work is the establishment of precise relations between these different definitions of normalized force and how they are related to commonly used drag laws. The drag laws developed based on PR DNS results of flow over a stationary random array of particles [2,3,6,7,9,10] are appropriate for application only as the Eulerian normalized average force $\Phi_0^E$, where the subscript 0 has been added to indicate its applicability for a stationary system of particles. The drag laws developed based on experiments on freely sedimenting particles [4,5,8] are appropriate as the Eulerian normalized average force $\Phi^E$. This however includes the added effect of particle-to-particle variation in the particle velocity and as a result $\Phi^E$ for nonstationary particles is typically larger than $\Phi_0^E$ and the difference depends on the magnitude of the particle-velocity variation.

While the Eulerian normalized average force correlation can be obtained from direct numerical simulations and experiments, the corresponding Lagrangian normalized force expressions cannot be directly obtained. Here we introduced the force consistency relation [see (32)] according to which $\Phi^L$, when properly defined and applied to each particle based on its relative velocity and volume fraction and averaged over all the particles within the averaging volume, must equal $\Phi^E$. Accordingly, while $\Phi^L$ is only a function of the particle's Reynolds number and volume fraction [as defined in (1)], $\Phi^E$ must be a function of not only the macroscale Reynolds number and volume fraction, but also of the particle-velocity variation Reynolds number (also rms volume fraction variation in the case of a nonuniform particle distribution).

A summary of all the Eulerian and Lagrangian force correlations discussed in this work is presented in Table II. The stationary limits presented in the second column are the limiting values

of those presented in the third column. We have used the drag correlation of Tenneti *et al.* [7] as an example of $\Phi_0^E$. It can be replaced with similar correlations advanced by others [2,3,6,9,10] and following the steps outlined in Sec. III the companion $\Phi_0^L$ can be derived so that they satisfy the force consistency relation. While the Lagrangian force correlation $\Phi^L$ and its stationary limit $\Phi_0^L$ depend only on $\mathrm{Re}_0$ and $\phi_0$, the EE and EL-mac correlations will additionally depend on the fluctuation Reynolds number that parametrizes particle-velocity variation. In the table it is assumed that in the EL-macro approach the filter length scale is sufficiently larger than the particle size so that it is essentially similar to the EE approach.

Finally, although the above drag correlations offer significant improvement over the use of the same standard drag in both the EL and EE simulations, several limitations can be identified. These limitations can be properly addressed with further research. (i) Free motion of particles will result in an inhomogeneous distribution of particles. The effect of volume fraction variation, in addition to particle-to-particle variation in the Reynolds number, must also be considered. This can be done in a similar manner. (ii) Equation (41) for the Eulerian force correlation is intended for broader use in a wide variety of EE and EL-mac simulations. However, its use requires knowledge of streamwise and transverse undisturbed fluid-velocity variation, particle-velocity variation, and their correlation. Such comprehensive knowledge is currently lacking. This requires further study with particle Stokes number (or particle-to-fluid density ratio) as an important parameter. (iii) Another fundamental assumption of the above approach is that the Lagrangian force correlation of an individual particle under the conditions of free motion, i.e., $\Phi^L$, has been taken to be the same as that under the stationary condition. This assumption is more appropriate than assuming $\Phi^E = \Phi_0^E$, since the former only ignores the secondary effect of neighbors on self-induced perturbation flow. This assumption of $\Phi^L = \Phi_0^L$ was required, since we do not know the perturbation flow in terms of superposable wakes under conditions of freely moving particles. Thus, establishing $\Phi^L$ under the conditions of freely moving particles will be an important future step. (iv) Here we have ignored the effect of particle rotation and the torque induced on the particle. The effects of particle rotation on both the particle force and torque variation have been studied [10,31,47] and these effects must be incorporated into future models.

## ACKNOWLEDGMENTS

## APPENDIX A: STRESS DIVERGENCE MAPS

Similar to the superposition given in (16), superposition applies to the microscale undisturbed pressure field as well

$$p_{\mathrm{mic,i}}(\boldsymbol{x}, t) \approx \sum_{j=1}^{N-1} p_{sw}(\boldsymbol{x} - \boldsymbol{x}_j; \mathrm{Re}_{@j}, \phi_{@j}). \tag{A1}$$

With the above definitions, the undisturbed velocity and pressure fields of each particle within the system can be explicitly calculated, but such a calculation as a sum over all the neighbors can be computationally expensive. In order to reduce the computational burden, we first note that $\boldsymbol{u}_{\mathrm{mic,i}}$ and

$p_{\text{mic,i}}$ are not needed in themselves in the force calculation. As seen in (14), in the evaluation of $\boldsymbol{F}_{\text{mic,un,i}}$ only the volume average is needed, which can be approximated as

$$\overline{(-\boldsymbol{\nabla} p_{\text{mic,i}} + \mu \nabla^2 \boldsymbol{u}_{\text{mic,i}})}^{V_i} \approx \sum_{j=1}^{N-1} \overline{(-\boldsymbol{\nabla} p_{sw} + \mu \nabla^2 \boldsymbol{u}_{sw})_j}^{V_i}, \tag{A2}$$

where $\overline{(\,)}_j^{V_i}$ stands for the stress divergence of the superposable wake of the $j$th particle being averaged over the volume occupied by the $i$th particle. Due to the axisymmetric nature of the superposable wake, this volume average depends only on the axial and radial distances between the $i$-$j$ particle pair, and on $\text{Re}_{@j}$ and $\phi_{@j}$, which determine the superposable wakes. Thus, in addition to the superposable wake velocity fields, the above volume average of stress divergence can be precomputed and stored as axisymmetric maps for varying $\text{Re}_{@j}$ and $\phi_{@j}$. Once computed and stored, the appropriate volume average contribution from each neighbor can be read and summed over as given in the above summation.

## APPENDIX B: UNDISTURBED FLOW FORCE PARAMETRIZATION IN THE EL APPROACH

The macro portion of the undisturbed flow force $\boldsymbol{F}_{\text{mac,un,i}}$ can be readily evaluated from the macroscale velocity and pressure fields of the EL simulation [see the first term on the right-hand side of (14)]. If the macroscale flow is nearly homogeneous (or slowly varying in $\boldsymbol{x}$), then the viscous contribution is generally very small and can be ignored. Furthermore, in the absence of acceleration effects, the macroscale pressure gradient that drives the flow must exactly balance the net force on all the particles [7,41], which yields

$$-\boldsymbol{\nabla} p = \frac{\phi(\boldsymbol{x}, t) \boldsymbol{F}(\boldsymbol{x}, t)}{\mathcal{V}}. \tag{B1}$$

In the above $\mathcal{V}$ is the volume of a particle and $\boldsymbol{F}$ is the average force. Substituting the above in the expression for $\boldsymbol{F}_{\text{mac,un,i}}$ (14) and ignoring the negligible contribution from the viscous stress, we identify the relation in which, under nonaccelerating conditions, the macroscale undisturbed flow force on a particle is simply $\phi$ times the average force.

The micro portion of the undisturbed flow force, $\boldsymbol{F}_{\text{mic,un,i}}$, has generally been ignored in EL simulations. Even though the precise locations of all the neighboring particles are known in an EL simulation, $\boldsymbol{F}_{\text{mic,un,i}}$ has been ignored mainly due to the fact that a method to obtain the neighbor-induced microscale perturbation flow has been lacking. The pairwise interaction extended point-particle model provides a rational approximation in terms of the summation of superposable wakes of nearby neighbors. According to the PIEP model, $\boldsymbol{F}_{\text{mic,un,i}}$ can be evaluated in terms of the precomputed force maps as given by the sum (A2).

## APPENDIX C: MACRO UNDISTURBED FLOW FORCE PARAMETRIZATION IN THE EE APPROACH

The macro portion of the undisturbed flow force can be evaluated by spatially averaging the corresponding EL quantity to obtain

$$\frac{\mathcal{V}}{\phi_p} \int_{\Omega} G(\boldsymbol{x} - \boldsymbol{x}') I_p(\boldsymbol{x}', t)(-\boldsymbol{\nabla} p + \mu \nabla^2 \boldsymbol{u}) dV \approx \mathcal{V}(-\boldsymbol{\nabla} p + \mu \nabla^2 \boldsymbol{u}). \tag{C1}$$

Here $\boldsymbol{u}(\boldsymbol{x}, t)$ and $p(\boldsymbol{x}, t)$ are the macroscale velocity and pressure fields of the EE simulation. In obtaining the right-hand side it is assumed that the macroscale stress divergence is slowly varying and therefore can be moved out of the integral. As in the EL approach, under nonaccelerating conditions the macroscale undisturbed flow force on a particle is simply $\phi$ times the average force. In the EE approach it is not possible to evaluate the microscale undisturbed flow, since the precise locations and motion of the neighbors are unavailable.

## APPENDIX D: APPROXIMATION OF AVERAGE DRAG

Towards the goal of obtaining an approximate evaluation of the average drag over all the particles given in (30), we first rewrite it as

$$\frac{1}{N}\sum_{i=1}^{N}\underbrace{\frac{\mathrm{Re}_{@ix}}{\mathrm{Re}_0}(1.0 + 0.15\,\mathrm{Re}_{@i}^{0.687})}_{\hat{\Phi}},\tag{D1}$$

where $\mathrm{Re}_{@ix} = (\boldsymbol{u}_{@i}\cdot\boldsymbol{e}_x)d/\nu$ is Reynolds number based on the streamwise $x$ component of the undisturbed fluid velocity at the $i$th stationary particle and furthermore we have the relation $\mathrm{Re}_{@i}^2 = \mathrm{Re}_{@ix}^2 + \mathrm{Re}_{@iy}^2 + \mathrm{Re}_{@iz}^2$. We now expand in a Taylor series the function $\hat{\Phi}$ in the triplet variables $(\mathrm{Re}_{@ix}, \mathrm{Re}_{@iy}, \mathrm{Re}_{@iz})$ about the macroscale value of $(\mathrm{Re}_0, 0, 0)$ as

$$\hat{\Phi} = [\hat{\Phi}]_0 + \left[\frac{\partial\hat{\Phi}}{\partial\,\mathrm{Re}_{@ix}}\right]_0(\mathrm{Re}_{@ix} - \mathrm{Re}_0) + \left[\frac{\partial\hat{\Phi}}{\partial\,\mathrm{Re}_{@iy}}\right]_0\mathrm{Re}_{@iy} + \left[\frac{\partial\hat{\Phi}}{\partial\,\mathrm{Re}_{@iz}}\right]_0\mathrm{Re}_{@iz}$$
$$+ \left[\frac{\partial^2\hat{\Phi}}{\partial\,\mathrm{Re}_{@ix}^2}\right]_0\frac{(\mathrm{Re}_{@ix} - \mathrm{Re}_0)^2}{2} + \left[\frac{\partial^2\hat{\Phi}}{\partial\,\mathrm{Re}_{@iy}^2}\right]_0\frac{\mathrm{Re}_{@iy}^2}{2} + \left[\frac{\partial^2\hat{\Phi}}{\partial\,\mathrm{Re}_{@iz}^2}\right]_0\frac{\mathrm{Re}_{@iz}^2}{2} + \cdots, \tag{D2}$$

where the notation $[(\ )]_0$ indicates the quantity within the square brackets being evaluated at the macroscale state. The partial derivatives are then evaluated and the linear terms are ignored in anticipation that they make zero contribution when averaged over all the particles. With these we obtain

$$\hat{\Phi} = (1.0 + 0.15\,\mathrm{Re}_0^{0.687}) + \frac{0.15\times0.687}{2\,\mathrm{Re}_0^{1.313}}[1.687(\mathrm{Re}_{@ix} - \mathrm{Re}_0)^2 + 2\,\mathrm{Re}_{@iy}^2] + \cdots.\tag{D3}$$

As the final step we average this expression over all the particles. When carrying out the average, averages of $\mathrm{Re}_{@ix} - \mathrm{Re}_0$ and $\mathrm{Re}_{@iy}$ are zero and therefore these terms were ignored in Eq. (D3). We also recognize averages of $(\mathrm{Re}_{@ix} - \mathrm{Re}_0)^2$ and $\mathrm{Re}_{@iy}^2$ to be $\mathrm{Re}_{Tfx}^2$ and $\mathrm{Re}_{Tfy}^2$. We thus obtain the final result given in Eq. (31).

[1] J. Schwarzkopf, M. Sommerfeld, C. Crowe, and Y. Tsuji, *Multiphase Flows with Droplets and Particles* (CRC, Boca Raton, 2011).

[2] R. Beetstra, M. A. van der Hoef, and J. Kuipers, Drag force of intermediate Reynolds number flow past mono- and bidisperse arrays of spheres, AIChE J. **53**, 489 (2007).

[3] S. Bogner, S. Mohanty, and U. Rüde, Drag correlation for dilute and moderately dense fluid-particle systems using the lattice Boltzmann method, Int. J. Multiphase Flow **68**, 71 (2015).

[4] D. Gidaspow, *Multiphase Flow and Fluidization: Continuum and Kinetic Theory Descriptions* (Academic, New York, 1994).

[5] J. F. Richardson and W. N. Zaki, The sedimentation of a suspension of uniform spheres under conditions of viscous flow, Chem. Eng. Sci. **3**, 65 (1954).

[6] Y. Y. Tang, E. F. Peters, J. H. Kuipers, S. S. Kriebitzsch, and M. M. van der Hoef, A new drag correlation from fully resolved simulations of flow past monodisperse static arrays of spheres, AIChE J. **61**, 688 (2015).

[7] S. Tenneti, R. Garg, and S. Subramaniam, Drag law for monodisperse gas-solid systems using particle-resolved direct numerical simulation of flow past fixed assemblies of spheres, Int. J. Multiphase Flow **37**, 1072 (2011).

[8] C. Y. Wen and Y. H. Yu, Mechanics of fluidization, Chem. Eng. Prog. Sym. Ser. **62**, 100 (1966).

[9] A. A. Zaidi, T. Tsuji, and T. Tanaka, A new relation of drag force for high Stokes number monodisperse spheres by direct numerical simulation, Adv. Powder Technol. **25**, 1860 (2014).

[10] Q. Zhou and L. S. Fan, Direct numerical simulation of moderate-Reynolds-number flow past arrays of rotating spheres, Phys. Fluids **27**, 073306 (2015).

[11] G. Akiki, T. Jackson, and S. Balachandar, Pairwise interaction extended point-particle model for a random array of monodisperse spheres, J. Fluid Mech. **813**, 882 (2017).

[12] G. Akiki, W. Moore, and S. Balachandar, Pairwise-interaction extended point-particle model for particle-laden flows, J. Comput. Phys. **351**, 329 (2017).

[13] G. Akiki and S. Balachandar, Immersed boundary method with non-uniform distribution of Lagrangian markers for a non-uniform Eulerian mesh, J. Comput. Phys. **307**, 34 (2016).

[14] G. Akiki, T. Jackson, and S. Balachandar, Force variation within arrays of monodisperse spherical particles, Phys. Rev. Fluids **1**, 044202 (2016).

[15] L. He and D. Tafti, A supervised machine learning approach for predicting variable drag forces on spherical particles in suspension, Powder Technol. **345**, 379 (2019).

[16] T. Ma, Y. Yu, X. Chen, and Q. Zhou, Effect of anisotropic micro-structures on fluid-particle drag in low-Reynolds-number monodisperse gas-solid suspensions, AIChE J. **66**, e16910 (2020).

[17] W. Moore, S. Balachandar, and G. Akiki, A hybrid point-particle force model that combines physical and data-driven approaches, J. Comput. Phys. **385**, 187 (2019).

[18] A. Seyed-Ahmadi and A. Wachs, Microstructure-informed probabilistic model for hydrodynamic forces in particle-laden flows, Bull. Am. Phys. Soc. **64**, 2 (2019).

[19] E. Thiam, E. Masi, E. Climent, O. Simonin, and S. Vincent, Particle-resolved numerical simulations of the gas-solid heat transfer in arrays of random motionless particles, Acta Mech. **230**, 541 (2019).

[20] I. Iliopoulos, Y. Mito, and T. J. Hanratty, A stochastic model for solid particle dispersion in a nonhomogeneous turbulent field, Int. J. Multiphase Flow **29**, 375 (2003).

[21] S. Balachandar, K. Liu, and M. Lakhote, Self-induced velocity correction for improved drag estimation in Euler-Lagrange point-particle simulations, J. Comput. Phys. **376**, 160 (2019).

[22] M. Esmaily and J. A. K. Horwitz, A correction scheme for two-way coupled point-particle simulations on anisotropic grids, J. Comput. Phys. **375**, 960 (2019).

[23] T. Fukada, S. Takeuchi, and T. Kajishima, Estimation of fluid forces on a spherical particle for two-way coupling simulation based on the volume averaging, Int. J. Multiphase Flow **113**, 165 (2019).

[24] P. Gualtieri, F. Picano, G. Sardina, and C. M. Casciola, Exact regularized point particle method for multiphase flows in the two-way coupling regime, J. Fluid Mech. **773**, 520 (2015).

[25] J. A. K. Horwitz and A. Mani, Correction scheme for point-particle models applied to a nonlinear drag law in simulations of particle-fluid interaction, Int. J. Multiphase Flow **101**, 74 (2018).

[26] P. Ireland and O. Desjardins, Improving particle drag predictions in Euler-Lagrange simulations with two-way coupling, J. Comput. Phys. **338**, 405 (2017).

[27] K. Liu, M. Lakhote, and S. Balachandar, Self-induced temperature correction for inter-phase heat transfer in Euler-Lagrange point-particle simulation, J. Comput. Phys. **396**, 596 (2019).

[28] J. F. Poustis, J. M. Senoner, D. Zuzio, and P. Villedieu, Regularization of the Lagrangian point force approximation for deterministic discrete particle simulations, Int. J. Multiphase Flow **117**, 138 (2019).

[29] J. Capecelatro, O. Desjardins, and R. O. Fox, On fluid-particle dynamics in fully developed cluster-induced turbulence, J. Fluid Mech. **780**, 578 (2015).

[30] J. Capecelatro, O. Desjardins, and R. O. Fox, Strongly coupled fluid-particle flows in vertical channels. I. Reynolds-averaged two-phase turbulence statistics, Phys. Fluids **28**, 033306 (2016).

[31] G. Rubinstein, A. Ozel, X. Yin, J. Derksen, and S. Sundaresan, Lattice Boltzmann simulations of low-Reynolds-number flows past fluidized spheres: effect of inhomogeneities on the drag force, J. Fluid Mech. **833**, 599 (2017).

[32] M. G. Pai and S. Subramaniam, A comprehensive probability density function formalism for multiphase flows, J. Fluid Mech. **628**, 181 (2009).

[33] W. Moore and S. Balachandar, Lagrangian investigation of pseudo-turbulence in multiphase flow using superposable wakes, Phys. Rev. Fluids **4**, 114301 (2019).

[34] S. Kim and S. J. Karrila, *Microhydrodynamics: Principles and Selected Applications* (Courier, Chelmsford, 2013).

[35] S. Balachandar and J. Eaton, Turbulent dispersed multiphase flow, Annu. Rev. Fluid Mech. **42**, 111 (2010).

[36] M. Maxey and J. Riley, Equation of motion for a small rigid sphere in a nonuniform flow, Phys. Fluids **26**, 883 (1983).

[37] S. Balachandar, C. Moore, G. Akiki, and K. Liu, Particle-resolved Accuracy in Euler-Lagrange simulations of multiphase flow using machine learning and pairwise interaction extended point-particle (PIEP) approximation, Theoretical Computational Fluid Dynamics (2020), doi:10.1007/s00162-020-00538-8.

[38] J. Capecelatro and O. Desjardins, An Euler-Lagrange strategy for simulating particle-laden flows, J. Comput. Phys. **238**, 1 (2013).

[39] Z. Huang, H. Wang, Q. Zhou, and T. Li, Effects of granular temperature on inter-phase drag in gas-solid flows, Powder Technol. **321**, 435 (2017).

[40] S. Tenneti, R. Garg, C. M. Hrenya, R. O. Fox, and S. Subramaniam, Direct numerical simulation of gas-solid suspensions at moderate Reynolds number: Quantifying the coupling between hydrodynamic forces and particle velocity fluctuations, Powder Technol. **203**, 57 (2010).

[41] J. J. Wylie, D. L. Koch, and A. J. C. Ladd, Rheology of suspensions with high particle inertia and moderate fluid inertia, J. Fluid Mech. **480**, 95 (2003).

[42] S. H. L. Kriebitzsch, M. A. Van der Hoef, and J. A. M. Kuipers, Fully resolved simulation of a gas-fluidized bed: A critical test of DEM models, Chem. Eng. Sci. **91**, 1 (2013).

[43] Y. Tang, E. A. J. F. Peters, and J. A. M. Kuipers, Direct numerical simulations of dynamic gas-solid suspensions, AIChE J. **62**, 1958 (2016).

[44] V. Tavanashad, A. Passalacqua, R. O. Fox, and S. Subramaniam, Effect of density ratio on velocity fluctuations in dispersed multiphase flow from simulations of finite-size particles, Acta Mech. **230**, 469 (2019).

[45] S. Balachandar, A scaling analysis for point-particle approaches to turbulent multiphase flows, Int. J. Multiphase Flow **35**, 801 (2009).

[46] Y. Ling, M. Parmar, and S. Balachandar, A scaling analysis of added-mass and history forces and their coupling in dispersed multiphase flows, Int. J. Multiphase Flow **57**, 102 (2013).

[47] Q. Zhou and L. S. Fan, Direct numerical simulation of low-Reynolds-number flow past arrays of rotating spheres, J. Fluid Mech. **765**, 396 (2015).